Performance Analysis of Multirobot Cooperative Localization

Anastasios I. Mourikis, *Student Member, IEEE*, and Stergios I. Roumeliotis, *Member, IEEE*

***Abstract*—This paper studies the accuracy of position estimation for groups of mobile robots performing cooperative localization. We consider the case of teams comprised of possibly heterogeneous robots and provide analytical expressions for the upper bound on their expected positioning uncertainty. This bound is determined as a function of the sensors' noise covariance and the eigenvalues of the relative position measurement graph (RPMG), i.e., the weighted directed graph which represents the network of robot-to-robot exteroceptive measurements. The RPMG is employed as a key element in this analysis, and its properties are related to the localization performance of the team. It is shown that, for a robot group of a certain size, the maximum expected rate of uncertainty increase is *independent* of the accuracy and number of relative position measurements and depends only on the accuracy of the proprioceptive and orientation sensors on the robots. Additionally, the effects of changes in the topology of the RPMG are studied, and it is shown that, at steady-state, these reconfigurations do *not* inflict any loss in localization precision. Experimental data, as well as simulation results that validate the theoretical analysis, are presented.**

***Index Terms*—Cooperative localization (CL), Kalman filtering, multirobot localization, positioning accuracy, relative position measurement graph (RPMG), sensor sharing.**

I. Introduction

In ORDER for a multirobot team to coordinate while navigating autonomously within an area, all robots must be able to determine their positions with respect to a common frame of reference. Frequently, robots need to communicate in order to coordinate their efforts during the execution of a task (e.g., exploration [1], [2], object transportation [3], [4], structure assembly [5], [6], etc). By acquiring, transmitting, and processing relative position measurements and pertinent positioning information, groups of robots can leverage their communication resources to perform *cooperative localization* (CL) and improve the accuracy of their position estimates. The topic of CL has recently attracted the interest of many researchers (e.g., [7]–[9]), primarily due to the flexibility that sensor and actuator sharing provides when designing heterogeneous robot teams that communicate through wireless networks [10].

Manuscript received July 8, 2005; revised January 20, 2006. This paper was recommended for publication by Associate Editor D. Fox and Editors I. Walker and K. Lynch upon evaluation of the reviewers' comments. This work was supported in part by the University of Minnesota GiA Award, DTC, in part by the Jet Propulsion Laboratory under Grants 1248696 and 1251073, and in part by the National Science Foundation ITR, under Grant EIA-0324864. This paper was presented in part at the IEEE International Conference on Robotics and Automation, New Orleans, LA, April/May 2004.

The authors are with the Department of Computer Science and Engineering, University of Minnesota, Minneapolis, MN 55455 USA (e-mails: mourikis@cs.umn.edu; stergios@cs.umn.edu).

Digital Object Identifier 10.1109/TRO.2006.878957

Predicting the positioning performance of heterogeneous robot teams for the general case of multirobot CL, in which the number, quality, and type of measurements may vary over time, remains an open problem to this date. The advent of formal tools that will enable engineers to predict the localization performance of multirobot teams will significantly impact the process of designing such teams for accomplishing a specific mission. Our work aims at providing *analytical expressions* for assessing the positioning accuracy of heterogeneous robot groups. During the design phase, informed decisions based on these relations can guide the selection of the appropriate size of the robot group and the accuracy of their sensors for achieving the desired level of localization precision. This, in effect, will result in considerable gains in terms of design expenses, since employing costly and time consuming simulation and experimental trials for specifying the positioning accuracy of robot groups, can be avoided altogether, or, at least deferred until the end of the design phase for verification. Forming teams with the necessary number of robots and equipping them with the essential sensors will introduce additional savings by reducing the probability of failure due to unexpected positioning errors.

In [11] and [12], upper bounds on the localization uncertainty of a homogeneous group of N robots were derived by directly solving the continuous-time Riccati equation for the covariance of the errors in the position estimates. The results of that work constitute the first analytical assessment of the positioning accuracy of multirobot teams. However, the assumption of *homogeneity* and the requirement that *every* robot continuously measures the relative position of *all* other robots in the team, limit their applicability to small groups of identical robots. In realistic scenarios, limitations on computational resources and communication bandwidth, may prohibit the robots from transmitting and processing all measurements available at every time instant, and additionally, even teams comprised of identically built robots, may actually be heterogeneous, due to the inherent variability during the manufacturing of their sensors (cf. Section VI).

In this paper, we relax these assumptions and study the time evolution of the positioning uncertainty in *heterogeneous* robot teams, with *arbitrary* topology of the relative position measurement graph (RPMG). Specifically, in Section IV, we derive upper bounds on the *worst case*, as well as on the *average* covariance matrix of the robots' position estimates. One of the main results of this paper is that, in the absence of absolute position measurements, the rate of positioning uncertainty increase in the group of robots is *constant*, identical for all the robots, and *independent* of the topology of the RPMG. The primary factor in determining this rate is the quality of the robots' proprioceptive and orientation sensors, as well as the number of communi-

cating robots. It is shown that the rate of uncertainty increase is *smaller* than the rate the single best robot would attain, if it were localizing on its own (cf. Corollary 5), which indicates that the exchange of positioning information benefits all robots.

The connectivity of the RPMG affects the constant (time-invariant) part of the covariance matrix that describes the localization uncertainty of the group. A study of the properties of the time evolution of the position covariance matrix in Section V shows that a *temporary* reduction in the number of relative position measurements can only cause *temporary* loss of positioning accuracy. Moreover, the case in which absolute position information, e.g., GPS measurements, is available to some of the robots of the team, is studied (cf. Lemma 2). In this scenario, it is shown that even if *one* robot has access to absolute position measurements, the variance in *all* robots' position errors remains bounded, and depends on the topology of the RPMG.

In the following section, we outline the existing approaches to CL, and in Section III we present the formulation of the multirobot localization problem. In Sections IV and V, the main theoretical results of this paper are derived, namely bounds on the positioning uncertainty of CL, and their properties. In Section VI, experimental results that validate the theoretical analysis are presented, while extensive simulation results are analyzed in Section VII. Finally, in Section VIII, the conclusions of this work are drawn and future research directions are suggested.

II. Related Work

Previous work on multirobot CL has considered collaborative strategies primarily for improving pose tracking in the absence of landmarks. A system where relative position measurements were used for CL was first reported in [7]. A group of robots is divided into two separate teams with alternating roles. At each time instant, one team is in motion while the other one remains stationary and acts as a set of landmarks. The teams then exchange roles and this process continues until both reach their goal. Improvements over this system and optimal motion strategies are discussed in [13]–[15]. Similarly, in [16], only one robot moves, while the rest of a group of small-sized robots forms an equilateral triangle of localization beacons in order to update their pose estimates. Another implementation of this type of CL is described in [2], [8], [17], where a team of robots moves through the open space systematically mapping the environment. In [18], the authors present a CL technique based on virtual links between robots which remain within the field of view of their teammates.

All the aforementioned approaches that rely on robots acting as *portable landmarks* have the following limitations: 1) only one robot (or team) is allowed to move at any given time; and 2) the two robots (or teams) must maintain line-of-sight contact at all times. In addition to the use of robots as portable landmarks, *static landmarks* have also been employed for facilitating the localization of robot teams, in the context of cooperative simultaneous localization and mapping (C-SLAM). Since this paper focuses on featureless localization, we will not discuss this case further. For a thorough presentation of the related literature, the interested reader is referred to [19], where the Riccati recursion is employed for the study of the positioning accuracy of C-SLAM. The distinguishing difference between the work presented here and that of [19] is that in the latter case, a number of static landmarks are assumed to be always visible, which results in bounded uncertainty for the robots' position estimates at all times. This is in contrast to the case of CL, as shown in Section IV.

A different collaborative multirobot localization scheme is presented in [20] and [21]. The authors have extended the Monte Carlo localization algorithm [22] to the case of two robots that both possess a map of the area. When these robots detect each other, the combination of their belief functions improves the accuracy and convergence speed of global localization. The main limitation of this approach is that it can be applied only within known indoor environments. In addition, since information interdependencies are being ignored every time the two robots meet, this method can lead to overly optimistic position estimates. This issue is discussed in detail in [23]. At the cost of increased computational requirements, [24] treats the problem of not considering the correlation terms in Monte Carlo-based CL by introducing a dependency tree.

In [25] and [26], a maximum likelihood estimator is employed to process relative pose and odometric measurements recorded by the robots, and a solution for the robots' pose is derived by invoking numerical optimization. In contrast to this *batch* approach, a *recursive* estimator design is more often employed for CL, due to its lower computational complexity. In [27], a Kalman filter-based implementation of CL is described, where the effect of the orientation uncertainty in both the state propagation and the relative position measurements is ignored, resulting in a simplified distributed algorithm. In [9] and [28] a distributed Kalman filter pose estimator is presented. Every robot collects sensor data regarding its motion continuously and measures the relative pose of other robots intermittently. Positioning information is propagated through the team only during the update cycles, allowing the Kalman filter to be decomposed into a number of smaller communicating filters, one for each robot. In [23], it has been shown that when every robot senses and communicates with its colleagues at all times, every member of the group has less uncertainty about its position than the robot with the most accurate odometric sensors when localizing independently.

To the best of our knowledge, there exist only few cases in the literature where analysis of the uncertainty propagation has been considered in the context of CL. In [27], the improvement in localization accuracy is computed, after only a *single* update step, with respect to the previous values of position uncertainty. In this case, the robots' orientations are assumed to be perfectly known and no expressions are derived for the propagation of the localization uncertainty with respect to time or the accuracy of the odometric and relative position measurements. In [29], the authors studied, in simulation, the effect of different robot-tracker sensing modalities on the accuracy of CL. Statistical properties were derived from simulated results for groups of robots of increasing size, when only one robot moved at a time. A numerical optimization approach for determining the trajectories resulting in the minimum localization uncertainty for a group of robots has been proposed in [30]. In [11] and [31], a *complete* RPMG for a *homogeneous* robot group is assumed and upper bounds on the positioning uncertainty of the robots

are computed. In [12], experimental and simulation results are presented that validate the accuracy of these bounds.

We hereafter present the details of our approach for deriving analytical expressions for the localization performance of a group of cooperating robots. Our problem formulation follows that presented in our previous work [11], [12], extended to the general case of *arbitrary* RPMGs and *heterogeneous* groups of robots [32].

III. Problem Formulation

Consider a group of N robots that employs an extended Kalman filter (EKF) estimator to perform CL. *Proprioceptive* measurements (e.g., velocity) are integrated to propagate the state estimates, while *exteroceptive* measurements (e.g., robot-to-robot relative position measurements) are processed to update these estimates. In our formulation, we assume that each robot has access to measurements of its absolute orientation, and that an upper bound on the variance of these measurements can be *a priori* determined. This is the case, for example, when each robot is equipped with a heading sensor of limited accuracy (e.g., a compass [33], [34] or a sun sensor [35], [36]) that directly measures its orientation, or if the robots infer their orientation from measurements of the structure of the environment in their surroundings (e.g., from the direction of the walls when this is known *a priori*) [37]. Alternatively, absolute orientation measurements can be obtained by observing objects in the horizon [38], or equivalently, the vanishing points of sets of parallel lines [39].

The variance of the absolute orientation measurements that each robot receives defines an upper bound on each robot's orientation uncertainty. The availability of such a bound enables us to decouple the task of position estimation from that of orientation estimation, for the purpose of determining upper bounds on the performance of CL. Specifically, we formulate a state vector comprised of only the positions of the N robots, and the orientation estimates are used as inputs to the system, of which noise-corrupted observations are available. Clearly, the resulting EKF-based estimator is a suboptimal one, since the correlations that exist between the position and orientation estimates of the robots are discarded. Thus, by deriving an upper bound on the covariance of the estimates produced with this suboptimal, "position-only" estimator, we simultaneously determine an upper bound on the covariance of the position estimates that would result from using a "full-state" EKF estimator.

We should note here that the condition for bounded orientation uncertainty is satisfied in most cases in practice. If, instead, special care is not taken and the errors in the orientation estimates of the robots are allowed to grow unbounded, any EKF-based estimator of their position will eventually diverge [40]. The significance of having small orientation errors for the *consistency* of the EKF has also been demonstrated in [41] and [42]. Thus, the requirement for bounded orientation errors is *not* an artificially imposed assumption; it is essentially a *prerequisite* for performing EKF-based localization. In fact, if we can determine the maximum tolerable value of the orientation variance, so that the linearization errors are acceptably small, we can use this variance value in the derivations that follow.

Throughout this paper, we consider that all robots move constantly in a random fashion (i.e., no specific formation is assumed as is the case in [43] and [44]). At every time step, some (or all) robots record relative position measurements, and use this information to improve the position estimates for all members of the group. During each EKF update cycle, all exteroceptive measurements, as well as the current position estimates of the robots, must be available to the estimator [28]. Therefore, it is assumed that a communication network exists enabling all robots to transmit such information. These can then be fused either in a distributed scheme, or at a central fusion center.

A key element in this analysis is the RPMG, which is defined as a graph whose vertices represent robots in the group and its directed edges correspond to relative position measurements (Fig. 5). That is, if robot i measures the relative position of robot j, the RPMG contains a directed edge from vertex i to vertex j. In this work, we primarily consider the most challenging scenario where the absolute positions of the robots cannot be measured or inferred. The case where global positioning information is available to at least one of the robots in the group, is subsumed in our formulation and is treated as a special one.

A. Position Propagation

We first study the influx of uncertainty to the system, due to the noise in the odometric measurements of the robots. The discrete-time motion equations for the ith robot of the team are

$$x_i(k+1) = x_i(k) + V_i(k)\delta t \cos(\phi_i(k)) \quad (1)$$

$$y_i(k+1) = y_i(k) + V_i(k)\delta t \sin(\phi_i(k)) \quad (2)$$

where $V_i(k)$ denotes the robot's translational velocity at time k and δt is the sampling period. In the Kalman filter framework, the estimates of the robot's position are propagated using the measurements of the robot's velocity, $V_{m_i}(k)$, and the estimates of the robot's orientation, $\hat{\phi}_i(k)$

$$\hat{x}_{i_{k+1|k}} = \hat{x}_{i_{k|k}} + V_{m_i}(k)\delta t \cos\left(\hat{\phi}_i(k)\right)$$

$$\hat{y}_{i_{k+1|k}} = \hat{y}_{i_{k|k}} + V_{m_i}(k)\delta t \sin\left(\hat{\phi}_i(k)\right).$$

Clearly, these equations are time-varying and nonlinear due to the dependence on the robot's orientation. By linearizing (1) and (2), the error propagation equation for the robot's position is readily derived

$$\begin{aligned}\begin{bmatrix}\widetilde{x}_{i_{k+1|k}}\\ \widetilde{y}_{i_{k+1|k}}\end{bmatrix} &= I_2\begin{bmatrix}\widetilde{x}_{i_{k|k}}\\ \widetilde{y}_{i_{k|k}}\end{bmatrix}\\ &\quad + \begin{bmatrix}\delta t\cos\left(\hat{\phi}_i(k)\right) & -V_{m_i}(k)\delta t\sin\left(\hat{\phi}_i(k)\right)\\ \delta t\sin\left(\hat{\phi}_i(k)\right) & V_{m_i}(k)\delta t\cos\left(\hat{\phi}_i(k)\right)\end{bmatrix}\\ &\quad \times\begin{bmatrix}w_{V_i}(k)\\ \widetilde{\phi}_i(k)\end{bmatrix}\\ \Leftrightarrow\quad \widetilde{p}_{i_{k+1|k}} &= \Phi_i(k)\widetilde{p}_{i_{k|k}} + G_i(k)W_i(k)\end{aligned} \quad (3)$$

where $\widetilde{p}_i(k) = [\widetilde{x}_i(k)\ \ \widetilde{y}_i(k)]^T$ is the error in the ith robot's position estimate, $\Phi_i(k) = I_2$ is the state transition matrix[1]

[1]Throughout this paper, I_n denotes the $n \times n$ identity matrix, $\mathbf{1}_{m\times n}$ denotes the $m \times n$ matrix of ones, and $\mathbf{0}_{m\times n}$ denotes the $m \times n$ matrix of zeros.

for robot i, and $V_{m_i}(k) = V_i(k) - w_{V_i}(k)$ are the measurements of the translational velocity of the robot, contaminated by a white zero-mean noise process with known variance $\sigma^2_{V_i}$. In the previous expressions, $\hat{\phi}_i(k)$ is the estimate of the robot's orientation at time k. The errors in the orientation estimates, $\tilde{\phi}_i(k) = \phi_i(k) - \hat{\phi}_i(k)$ are modeled by a white zero-mean noise process, whose variance, $\sigma^2_{\phi_i} = E\{\tilde{\phi}_i^2\}$, is bounded.

The covariance function of the system noise affecting the ith robot is

$$\begin{aligned} Q_i(k,k') &= E\left\{G_i(k)W_i(k)W_i(k')^T G_i(k')^T\right\} \\ &= C\left(\hat{\phi}_i(k)\right)\begin{bmatrix}\delta t^2\sigma^2_{V_i} & 0\\ 0 & \delta t^2\sigma^2_{\phi_i}V^2_{m_i}\end{bmatrix} C^T\left(\hat{\phi}_i(k)\right)\delta_{kk'} \\ &= C^T\left(\hat{\phi}_i(k)\right) Q_{d_i} C\left(\hat{\phi}_i(k)\right)^T \delta_{kk'} \end{aligned} \tag{4}$$

where $\delta_{kk'}$ is the Kronecker delta function, and $C(\hat{\phi}_i(k))$ is the 2×2 rotation matrix associated with $\hat{\phi}_i(k)$.

The state vector for the entire system is defined as the stacked vector comprised of the positions of the N robots, i.e.,

$$X(k) = \begin{bmatrix} p_1^T(k) & p_2^T(k) & \cdots & p_N^T(k)\end{bmatrix}^T.$$

Hence, the state transition matrix for the entire system at time step k is $\mathbf{\Phi}_k = I_{2N}$, and since the errors in the odometric measurements of the robots are uncorrelated, the covariance matrix of the system noise is given by

$$\mathbf{Q}(k) = \begin{bmatrix} Q_1(k,k) & \cdots & \mathbf{0}_{2\times 2} \\ \vdots & \ddots & \vdots \\ \mathbf{0}_{2\times 2} & \cdots & Q_N(k,k)\end{bmatrix} = \mathbf{Diag}\left(Q_i(k,k)\right) \tag{5}$$

where $\mathbf{Diag}(\cdot)$ denotes a block diagonal matrix. The equation for propagating the covariance matrix of the state error is written as

$$\mathbf{P}_{k+1|k} = \mathbf{P}_{k|k} + \mathbf{Q}(k) \tag{6}$$

where $\mathbf{P}_{k+1|k} = E\{\tilde{X}_{k+1|k}\tilde{X}^T_{k+1|k}\}$ and $\mathbf{P}_{k|k} = E\{\tilde{X}_{k|k}\tilde{X}^T_{k|k}\}$ are the covariance of the error in the estimate of $X(k+1)$ and $X(k)$, respectively, after all measurements up to time k have been processed.

B. Exteroceptive Measurement Model

1) Relative Position Measurements: At this point, we consider the exteroceptive measurements that the robots process to update their position estimates. The relative position measurement z_{ij} between robot i and j at time instant k is defined as

$$\begin{aligned} z_{ij}(k) &= C^T\left(\phi_i(k)\right)\left(p_j(k) - p_i(k)\right) + n_{z_{ij}}(k) \\ &= C^T\left(\phi_i(k)\right)\Delta p_{ij}(k) + n_{z_{ij}}(k) \end{aligned} \tag{7}$$

where $n_{z_{ij}}(k)$ is a white zero-mean noise process affecting the measurement. By linearizing (7), the measurement error is obtained:

$$\begin{aligned} \tilde{z}_{ij}(k) &= z_{ij}(k) - \hat{z}_{ij}(k) \\ &\simeq H_{ij}(k)\tilde{X}(k) + \Gamma_{ij}(k)n_{ij}(k) \end{aligned}$$

where

$$H_{ij}(k) = C^T\left(\hat{\phi}_i(k)\right)H_{o_{ij}} \tag{8}$$

$$H_{o_{ij}} = \begin{bmatrix}\mathbf{0}_{2\times 2} & \cdots & \underbrace{-I_2}_{i} & \cdots & \underbrace{I_2}_{j} & \cdots & \mathbf{0}_{2\times 2}\end{bmatrix}$$

$$\tilde{X}(k) = \begin{bmatrix}\tilde{p}_1^T(k) & \cdots & \tilde{p}_i^T(k) & \cdots & \tilde{p}_j^T(k) & \cdots & \tilde{p}_N^T(k)\end{bmatrix}^T$$

$$\Gamma_{ij}(k) = \begin{bmatrix} I_2 & -C^T\left(\hat{\phi}_i(k)\right)J\widehat{\Delta p}_{ij}(k)\end{bmatrix}$$

$$J = \begin{bmatrix}0 & -1\\ 1 & 0\end{bmatrix}, \quad n_{ij}(k) = \begin{bmatrix} n_{z_{ij}}(k) \\ \tilde{\phi}_i(k)\end{bmatrix}$$

$$\widehat{\Delta p}_{ij}(k) = \hat{p}_j(k) - \hat{p}_i(k). \tag{9}$$

The covariance for the measurement error is given by

$$\begin{aligned} {}^iR_{ij}(k) &= \Gamma_{ij}(k)E\left\{n_{ij}(k)n_{ij}^T(k)\right\}\Gamma_{ij}^T(k) \\ &= E\left\{n_{z_{ij}}n_{z_{ij}}^T\right\} + \sigma^2_{\phi_i}C^T(\hat{\phi}_i)J\widehat{\Delta p}_{ij}\widehat{\Delta p}_{ij}^T J^T C(\hat{\phi}_i) \\ &= {}^iR_{z_{ij}} + {}^iR_{\tilde{\phi}_{ij}} \end{aligned} \tag{10}$$

where time arguments have been dropped for simplicity of notation. This expression encapsulates all sources of noise and uncertainty that contribute to the measurement error $\tilde{z}_{ij}(k)$. More specifically, ${}^iR_{z_{ij}}(k)$ is the covariance of the noise $n_{z_{ij}}(k)$ in the recorded relative position measurement $z_{ij}(k)$ and ${}^iR_{\tilde{\phi}_{ij}}(k)$ is the additional covariance term due to the error $\tilde{\phi}_i(k)$ in the orientation estimate $\hat{\phi}_i(k)$ of the observing robot i.

Assuming that each relative position measurement consists of a range measurement ρ_{ij} and a bearing measurement θ_{ij}, whose errors $n_{\rho_{ij}}$ and $n_{\theta_{ij}}$ are uncorrelated, the term ${}^iR_{z_{ij}}(k)$ can be expressed as [45]

$${}^iR_{z_{ij}}(k) = C\left(\hat{\theta}_{ij}(k)\right)\begin{bmatrix}\sigma^2_{\rho_i} & 0\\ 0 & \hat{\rho}^2_{ij}(k)\sigma^2_{\theta_i}\end{bmatrix} C^T\left(\hat{\theta}_{ij}(k)\right) \tag{11}$$

where σ_{ρ_i} and σ_{θ_i} are the standard deviations of the white zero-mean noise processes affecting the range and bearing measurements of robot i, respectively. Here, it is assumed that all relative position measurements performed by one robot are corrupted by noise of equal variance. This assumption is employed merely to simplify the presentation, since it is not necessary in the derivations that follow. $C(\hat{\theta}_{ij}(k))$ is the rotational matrix associated with the bearing angle of the relative position measurement, expressed in the robot's coordinate frame.

Due to the existence of the common error component attributed to $\tilde{\phi}_i(k)$, the measurements that each robot performs

are correlated. The matrix of correlation between the errors in the measurements $z_{ij}(k)$ and $z_{i\ell}(k)$ received by robot i is

$$\begin{aligned} {}^iR_{j\ell}(k) &= \Gamma_{ij}(k) E\left\{n_{ij}(k) n_{i\ell}^T(k)\right\} \Gamma_{i\ell}^T(k) \\ &= \sigma_{\phi_i}^2 C^T\left(\hat{\phi}_i\right) J\widehat{\Delta p}_{ij} \widehat{\Delta p}_{i\ell}^T J^T C\left(\hat{\phi}_i\right). \end{aligned} \quad (12)$$

The results of (10)–(12) allow for the evaluation of the $2M_i \times 2M_i$ covariance matrix $\boldsymbol{R}_i(k)$ of all the M_i relative position measurements gathered by robot i at each time instant. This is a matrix whose 2×2 block diagonal elements equal ${}^iR_{ij}(k)$, $j \in \mathcal{N}_{M_i} \subset \{1, \ldots, N\} \setminus \{i\}$, where $\mathcal{N}_{M_i}$ is the set of the indices of the robots j observed by robot i. The off-diagonal block elements of $\boldsymbol{R}_i(k)$ are ${}^iR_{j\ell}(k)$, $j, \ell \in \mathcal{N}_{M_i}, j \neq \ell$. It can be shown that [45]

$$\boldsymbol{R}_i(k) = \boldsymbol{\Xi}_{\hat{\phi}_i}^T \boldsymbol{R}_{o_i}(k) \boldsymbol{\Xi}_{\hat{\phi}_i} \quad (13)$$

where $\boldsymbol{\Xi}_{\hat{\phi}_i} = I_{M_i} \otimes C(\hat{\phi}_i)$, with $\otimes$ denoting the Kronecker matrix product, and

$$\begin{aligned} \boldsymbol{R}_{o_i}(k) = \sigma_{\rho_i}^2 I_{2M_i} - D_i \mathrm{diag}\left(\frac{\sigma_{\rho_i}^2}{\hat{\rho}_{ij}^2}\right) D_i^T + \sigma_{\theta_i}^2 D_i D_i^T \\ + \sigma_{\phi_i}^2 D_i \mathbf{1}_{M_i \times M_i} D_i^T. \end{aligned} \quad (14)$$

In this last expression, $D_i = \mathbf{Diag}(J\widehat{\Delta p}_{ij})$ is the block diagonal matrix with diagonal elements $J\widehat{\Delta p}_{ij}$, $j \in \mathcal{N}_{M_i}$. It is interesting to note that the term $\boldsymbol{R}_{o_i}(k)$ is *independent* of the robots' orientations.

The measurement matrix describing the relative position measurements performed by robot i at each time step is a matrix whose block rows are H_{ij}, $j \in \mathcal{N}_{M_i}$, i.e.,

$$\boldsymbol{H}_i(k) = \boldsymbol{\Xi}_{\hat{\phi}_i}^T \boldsymbol{H}_{o_i} \quad (15)$$

where $\boldsymbol{H}_{o_i}$ is a *constant* matrix with block rows $H_{o_{ij}}$, $j \in \mathcal{N}_{M_i}$ [cf. (9)].

The measurement matrix for the entire system $\mathbf{H}(k)$ is defined as the block matrix with block rows $\boldsymbol{H}_i(k)$. Since the measurements performed by different robots are independent, the associated covariance matrix, $\mathbf{R}(k)$, is a block diagonal matrix with elements $\boldsymbol{R}_i(k)$ [cf. (13)]. The covariance update equation of the EKF is written as

$$\begin{aligned} \mathbf{P}_{k+1|k+1} = \mathbf{P}_{k+1|k} \\ - \mathbf{P}_{k+1|k} \mathbf{H}^T(k+1) \mathbf{S}^{-1}(k+1) \mathbf{H}(k+1) \mathbf{P}_{k+1|k} \end{aligned}$$

with $\mathbf{S}(k+1) = \mathbf{H}(k+1)\mathbf{P}_{k+1|k}\mathbf{H}^T(k+1) + \mathbf{R}(k+1)$. Substitution from (13) and (15) and simple algebraic manipulation leads to the orientation-dependent terms being cancelled out, and yields the expression

$$\mathbf{P}_{k+1|k+1} = \mathbf{P}_{k+1|k} - \mathbf{P}_{k+1|k} \mathbf{H}_o^T \mathbf{S}_o(k+1)^{-1} \mathbf{H}_o \mathbf{P}_{k+1|k} \quad (16)$$

with $\mathbf{S}_o(k+1) = \mathbf{H}_o \mathbf{P}_{k+1|k} \mathbf{H}_o^T + \mathbf{R}_o(k+1)$. In these equations, $\mathbf{R}_o$ is a block diagonal matrix with elements $\boldsymbol{R}_{o_i}$ while $\mathbf{H}_o$ is a matrix whose block rows are $\boldsymbol{H}_{o_i}$ [cf. (14)]. Considering the structure of the measurement equations leads to the observation that the matrix $\mathbf{H}_o$ can be written as $\mathbf{H}_o = H_o \otimes I_2$ where H_o is the *incidence matrix* of the RPMG describing the relative position measurements that are recorded at each time step. This indicates the close connection between the structure of the RPMG and the equations describing the time evolution of the positioning uncertainty during CL (see also Section IV-A.2 for a more thorough investigation of this relationship). Note that, since the sum of the elements of each row of H_o is equal to zero, we can write

$$\begin{aligned} H_o \mathbf{1}_{N\times 1} = \mathbf{0}_{N\times 1} \Rightarrow \\ \mathbf{H}_o \left(\mathbf{1}_{N\times 1} \otimes I_2\right) = \mathbf{0}_{2N\times 2} \Rightarrow \\ \mathbf{H}(k) \left(\mathbf{1}_{N\times 1} \otimes I_2\right) = \mathbf{0}_{2N\times 2}. \end{aligned} \quad (17)$$

Using this result, it is trivial to show that the system is not observable (intuitively, this means that any displacement of the entire robot team with respect to the origin of the global coordinate frame can not be detected). Additionally, it is clear that a basis of the unobservable subspace is formed by the columns of the matrix $V = \mathbf{1}_{N\times 1} \otimes I_2$. This observation will be useful in the analysis of the following section.

2) Absolute Position Measurements: Up to this point, only relative position measurements have been considered. If any of the robots, e.g., robot n has access to absolute positioning information, such as GPS measurements or from a map of the area, the corresponding submatrix element of $\mathbf{H}(k)$ is

$$H_{a_n} = \begin{bmatrix} \mathbf{0}_{2\times 2} & \ldots & \underbrace{I_2}_{n} & \ldots & \mathbf{0}_{2\times 2} \end{bmatrix} \quad (18)$$

while $\mathbf{R}_{a_n}$, the covariance of the absolute position measurement, is a constant provided by the specifications of the absolute positioning sensor. To account for the absolute position measurements, the matrix $\mathbf{H}_o$ in (16) is augmented by simply appending the appropriate block rows $\boldsymbol{H}_{a_n}$, while $\mathbf{R}_o$ is augmented by appending the matrices $\mathbf{R}_{a_n}$ on the diagonal, yielding

$$\mathbf{R}_o(k) = \begin{bmatrix} \mathbf{Diag}\left(\boldsymbol{R}_{o_i}(k)\right) & \mathbf{0} \\ \mathbf{0} & \mathbf{Diag}\left(\mathbf{R}_{a_n}\right) \end{bmatrix}. \quad (19)$$

IV. Riccati Recursion

In the preceding section, the covariance propagation and update equations for the position estimates of the robot team have been derived. Combining these two equations, by substituting the expression from (16) into (6), yields the Riccati recursion, which describes the time evolution of the covariance during CL. The resulting expression is

$$\begin{aligned} \mathbf{P}_{k+1} = \mathbf{P}_k - \mathbf{P}_k \mathbf{H}_o^T \left(\mathbf{H}_o \mathbf{P}_k \mathbf{H}_o^T + \mathbf{R}_o(k+1)\right)^{-1} \mathbf{H}_o \mathbf{P}_k \\ + \mathbf{Q}(k+1) \end{aligned} \quad (20)$$

where the substitutions $\mathbf{P}_k = \mathbf{P}_{k+1|k}$ and $\mathbf{P}_{k+1} = \mathbf{P}_{k+2|k+1}$ have been introduced to simplify the notation. The initial value of this recursion $\mathbf{P}_0$ is equal to the initial covariance matrix of the team's position estimates. It should be noted that the above recursion is obtained under the assumption that both odometric

and exteroceptive measurements are processed at the same rate. However, this is not always the case, since odometric data are commonly available at a higher rate. To address this problem a *continuous-time* analysis of the time-evolution of the covariance has also been conducted [45].

A. Upper Bound on Steady-State Covariance

We note that the matrices $\mathbf{Q}(k+1)$ and $\mathbf{R}_o(k+1)$ in (20) are time-varying, and thus, a closed-form solution to the Riccati recursion for $\mathbf{P}_k$ cannot be derived in the general case. However, by exploiting the monotonicity and concavity properties of the Riccati recursion, we are able to derive *upper bounds* for the *worst case*, as well as for the *expected* covariance of the position estimates during CL. These are the main results of the paper and are presented in the following.

Specifically, we are interested in characterizing the time-evolution of the uncertainty at *steady-state*, i.e., after sufficient time has elapsed for the transient phenomena in the solution of (20) to subside. It can be shown [45] that the right-hand side of the Riccati recursion is a matrix-increasing function of the covariance matrices $\mathbf{Q}(k+1)$ and $\mathbf{R}_o(k+1)$, as well as of the state covariance matrix $\mathbf{P}_k$. These properties allow us to prove the following lemma [45].

Lemma 1: If $\mathbf{R}_u$ and $\mathbf{Q}_u$ are matrices such that $\mathbf{R}_u \succeq \mathbf{R}_o(k+1)$ and $\mathbf{Q}_u \succeq \mathbf{Q}(k+1)$, for all $k \geq 0$, then the solution to the Riccati recursion

$$\mathbf{P}^u_{k+1} = \mathbf{P}^u_k - \mathbf{P}^u_k\mathbf{H}_o^T\left(\mathbf{H}_o\mathbf{P}^u_k\mathbf{H}_o^T + \mathbf{R}_u\right)^{-1}\mathbf{H}_o\mathbf{P}^u_k + \mathbf{Q}_u \quad (21)$$

with the initial condition $\mathbf{P}^u_0 = \mathbf{P}_0$, satisfies $\mathbf{P}^u_k \succeq \mathbf{P}_k$ for all $k \geq 0$.

From this lemma, we conclude that if we obtain upper bounds for the covariance of the system and measurement noise, we can formulate a *constant coefficient* Riccati recursion, whose solution is an upper bound on the covariance of the position estimates in CL. This recursion describes the time evolution of the covariance of a deduced linear time invariant (LTI) system whose measurements' covariance is *larger or equal* to the covariance of the measurements in the actual, nonlinear and time-varying, system.[2]

An upper bound for $\mathbf{Q}(k+1)$ is derived by noting that since $C(\hat{\phi}_i)$ is an orthonormal matrix, the eigenvalues of $Q_i(k+1, k+1)$ are equal to $\delta t^2\sigma^2_{V_i}$ and $\delta t^2\sigma^2_{\phi_i}V^2_{m_i}$ [cf. (4)]. Assuming that the maximum velocity of robot i is equal to $V_{\max}$, we denote

$$q_i = \max\left(\delta t^2\sigma^2_{V_i}, \delta t^2 V^2_{\max}\sigma^2_{\phi_i}\right). \quad (22)$$

This definition states that q_i is the maximum eigenvalue of $Q_i(k+1, k+1)$ and therefore

$$Q_i(k+1,k+1) \preceq q_i I_2 \Rightarrow \mathbf{Q}(k+1) \preceq \mathbf{Diag}(q_i I_2) = \mathbf{Q}_u.$$

[2]We note at this point that a similar result was derived, for the continuous-time case, by Nishimura in [46]. In that work, the author addresses the issue of designing Kalman filter (KF) estimators for *linear* systems for which the initial state covariance matrix, as well as the covariance of the measurements, is unknown. It is shown that, if the covariance values that are employed in the KF are inflated estimates of the true covariance matrices, then the filter remains consistent.

An upper bound for $\mathbf{R}_o(k+1)$ can be derived by considering the maximum distance, ρ_o, at which relative position measurements can be recorded by robot i. This distance can, for example, be determined by the maximum range of the robots' relative position sensors, or, by the size of the area in which the robots operate. In Appendix I, it is shown that

$$\mathbf{R}_{o_i}(k+1) \preceq \left(\sigma^2_{\rho_i} + M_i\sigma^2_{\phi_i}\rho^2_o + \sigma^2_{\theta_i}\rho^2_o\right) I_{2M_i} = r_i I_{2M_i}$$

and thus, an upper bound on $\mathbf{R}_o(k+1)$ is computed as

$$\mathbf{R}_o(k+1) \preceq \mathbf{R}_u = \begin{bmatrix} \mathbf{Diag}\left(r_i I_{2M_i}\right) & \mathbf{0} \\ \mathbf{0} & \mathbf{Diag}\left(\mathbf{R}_{a_n}\right) \end{bmatrix}. \quad (23)$$

We note at this point that the upper bounds derived in the preceding expressions are valid only for the particular sensor models employed in this paper. However, the approach is valid for *any* sensor model, as long as it is possible to determine appropriate upper bounds on the measurement and system noise covariance matrices. For example, a holonomic kinematic model could be employed instead of the nonholonomic model in (1) and (2), and the more accurate method of evaluating the covariance of the relative position measurements of Lerro and Bar-Shalom [47] could be employed in (11).

Having derived upper bounds for $\mathbf{Q}(k+1)$ and $\mathbf{R}_o(k+1)$, mere substitution in (21) and numerical evaluation of the solution to the resulting recursion, yields an upper bound on the maximum possible uncertainty of the position estimates in CL, at any time instant after the deployment of the robot team. However, significant insight on the properties of the covariance matrix can be gained by evaluating the solution of (21) at steady-state. In order to compute the steady-state solution for $\mathbf{P}^u_k$, we first apply the matrix inversion lemma to obtain

$$\begin{aligned}\mathbf{P}^u_{k+1} &= \mathbf{P}^u_k - \mathbf{P}^u_k\mathbf{H}_o^T\left(\mathbf{H}_o\mathbf{P}^u_k\mathbf{H}_o^T + \mathbf{R}_u\right)^{-1}\mathbf{H}_o\mathbf{P}^u_k + \mathbf{Q}_u \\ &= \mathbf{P}^u_k\left(I_{2N} + \mathbf{H}_o^T\mathbf{R}_u^{-1}\mathbf{H}_o\mathbf{P}^u_k\right)^{-1} + \mathbf{Q}_u. \end{aligned} \quad (24)$$

The derivations are simplified by defining the *normalized* covariance matrix as $\mathbf{P}_{n_k} = \mathbf{Q}_u^{-1/2}\mathbf{P}^u_k\mathbf{Q}_u^{-1/2}$, thus yielding

$$\mathbf{P}_{n_{k+1}} = \mathbf{P}_{n_k}\left(I_{2N} + \mathbf{C}_u\mathbf{P}_{n_k}\right)^{-1} + I_{2N} \quad (25)$$

where $\mathbf{C}_u = \mathbf{Q}_u^{1/2}\mathbf{H}_o^T\mathbf{R}_u^{-1}\mathbf{H}_o\mathbf{Q}_u^{1/2}$. Note that the only parameter in the above Riccati recursion is matrix $\mathbf{C}_u$, which contains the main parameters that characterize the localization performance of the robotic team. The eigenvalues of this matrix are in close relation with the type and number of exteroceptive measurements recorded by the robots of the team, and determine the properties of the upper bound on the steady-state positioning uncertainty. In [45], it is shown that when at least one robot of a team performing CL has access to absolute positioning information, matrix $\mathbf{C}_u$ is nonsingular. In contrast, when the robots of the team only record relative position measurements, this matrix is singular and has two eigenvalues equal to zero. These proofs are straightforward, when the rank of $\mathbf{H}_o$ is considered. We hereafter present the uncertainty bounds for two distinct cases, based on the availability of absolute positioning information.

1) Observable System: If at least one of the robots receives absolute position measurements then from a control theoretic perspective the system is observable, and the covariance of the position estimates for the robots remains bounded at steady-state [28]. An upper bound for the steady-state covariance of CL in this case is determined by the asymptotic solution of the Riccati recursion in (25). This derivation is presented in Appendix II, and the final result is stated as a lemma.

Lemma 2: The steady-state covariance of the position estimates for a team of robots performing CL, when at least one robot has access to absolute positioning information is bounded above by the matrix

$$\mathbf{P}_{ss}^{u} = \mathbf{Q}_u^{1/2}\mathbf{U}\mathbf{diag}\left(\frac{1}{2}+\sqrt{\frac{1}{4}+\frac{1}{\lambda_i}}\right)\mathbf{U}^T\mathbf{Q}_u^{1/2} \tag{26}$$

where we have denoted the singular value decomposition of $\mathbf{C}_u$ as $\mathbf{C}_u = \mathbf{U}\mathrm{diag}(\lambda_i)\mathbf{U}^T$.

At this point, we should note that the upper bound on the steady-state uncertainty depends on the topology of the RPMG (affecting $\mathbf{C}_u$) and the accuracy of the proprioceptive and exteroceptive sensors of the robots, represented by $\mathbf{Q}_u$ and $\mathbf{R}_u$, which are "embedded" in $\mathbf{C}_u$. However, the steady-state uncertainty is independent of the initial covariance of the robots, which comes as no surprise, since the system is observable.

2) Unobservable System: If none of the robots receives absolute position measurements, the system is unobservable, from a control theoretic perspective, and thus, the steady state uncertainty for the robots' position estimates will be a monotonically increasing function of time. In this case, the upper bound on the steady state covariance of the position estimates is described by the following lemma, whose proof is presented in Appendix II.

Lemma 3: When none of the robots of the team has access to absolute position measurements, the positioning uncertainty of CL at steady-state is bounded above by

$$\begin{aligned}\mathbf{P}_{ss}^{u}(k) = {} & k\cdot q_T\mathbf{1}_{N\times N}\otimes I_2 + \mathbf{Q}_u^{1/2}\mathbf{U} \\ & \times\begin{bmatrix}\mathbf{diag}_\xi\left(\frac{1}{2}+\sqrt{\frac{1}{4}+\frac{1}{\lambda_i}}\right) & \mathbf{0}_{\xi\times 2}\\ \mathbf{0}_{2\times\xi} & \mathbf{0}_{2\times 2}\end{bmatrix}\mathbf{U}^T\mathbf{Q}_u^{1/2} \\ & + q_T\mathbf{1}_{N\times N}\otimes\begin{bmatrix}\alpha & \beta\\ \gamma & \delta\end{bmatrix}\end{aligned} \tag{27}$$

where λ_i, $i = 1\ldots 2N-2$ are the nonzero singular values of $\mathbf{C}_u$, $\xi = 2N-2$ is the dimension of the diagonal submatrix appearing in the preceding expression, q_T is defined as

$$\frac{1}{q_T} = \sum_{i=1}^{N}\frac{1}{q_i} \tag{28}$$

and the parameters $\alpha, \beta, \gamma, \delta$ are defined as follows. Let

$$W = q_T\mathbf{Q}_u^{-1}(I_{2N}+\mathbf{P}_0\mathbf{Q}_u^{-1/2}h(\mathbf{C}_u)\mathbf{Q}_u^{-1/2})^{-1}\mathbf{P}_0\mathbf{Q}_u^{-1}$$

where

$$h(\mathbf{C}_u) = \mathbf{U}\,\mathrm{diag}\left(\frac{\lambda_i}{2}+\sqrt{\frac{\lambda_i^2}{4}+\lambda_i}\right)\mathbf{U}^T.$$

Then, $\alpha = \sum_{i,j\ \mathrm{odd}} w_{ij}$ ($\delta = \sum_{i,j\ \mathrm{even}} w_{ij}$) is the sum of all elements of $W = [w_{ij}]$ with two odd (even) indices and $\gamma = \sum_{i\ \mathrm{odd},j\ \mathrm{even}} w_{ij}$ is the sum of all elements of $W = [w_{ij}]$ with an odd row index and an even column index. Due to symmetry, $\beta = \gamma$.

Several observations can be made with respect to the above result. We note that the upper bound comprises three terms, the first of which contributes with a *constant rate* of uncertainty increase that is equal to $q_T\delta t^{-1}$. The second term in (27) is a constant term, whose value depends on the *topology* of the RPMG and the *accuracy* of the sensors on the robots. Finally, the third term in (27) is a constant term that describes the effect of the *initial uncertainty* on the steady-state covariance. It also depends on the noise characteristics of the sensors of the robots, as well as the RPMG topology. The fact that the steady-state bound depends on the initial uncertainty is a consequence of the fact that the system is *not* observable, and therefore, initial errors in the estimates for the robots' positions cannot be fully compensated for.

It is clear that the most important term in (27) is the one that corresponds to a *constant rate* of uncertainty increase. After sufficient time, this term will always dominate the remaining ones, and will largely determine the worst-case positioning performance of the team. A striking observation is that q_T, the rate of increase of the maximum uncertainty, is *independent* of both the topology of the RPMG and of the precision of the robots' relative position measurements. This quantity depends solely on the number of robots in the team, and the accuracy of the robots' dead reckoning (DR) capabilities [cf. (22)]. An intuitive interpretation of this result is that the primary factor determining the rate of uncertainty increase is the rate at which uncertainty is injected in the unobservable subspace of the system. Since the number, or the accuracy, of the relative position measurements does not alter this subspace, we should expect no change in the rate of uncertainty increase, as a result of changes in the information contributed by the exteroceptive measurements.

Further insight into the properties of the covariance matrix in CL can be gained by studying the effects of the RPMG topology on the eigenvalues of $\mathbf{C}_u$. For simplicity, we examine here the case where all robots receive odometry measurements of equal accuracy (i.e., $q_i = q$, for $i = 1,\ldots,N$). Employing the results of (9) and (23), the matrix $\mathbf{C}_u$ can, thus, be written as

$$\mathbf{C}_u = q\left(H_o^T\mathbf{Diag}\left(r_i^{-1}I_{M_i}\right)H_o\right)\otimes I_2 = q\mathcal{L}\otimes I_2. \tag{29}$$

As discussed earlier, H_o is the *incidence matrix* of the RPMG and therefore, $H_o\mathbf{Diag}(r_i^{-1/2}I_{M_i})$ is the incidence matrix of the *weighted* RPMG, where each edge is assigned weight proportional to the accuracy of the corresponding measurement. With this definition, we see that the matrix $\mathcal{L}$ is the *Laplacian matrix* of the weighted RPMG [48], and the eigenvalues of $\mathbf{C_u}$ are given by [cf. (29)]

$$\lambda_{2k-1} = \lambda_{2k} = q\lambda_{\mathcal{L}_k},\quad k = 1,\ldots,N \tag{30}$$

where $\lambda_{\mathcal{L}_k}$, $k = 1,\ldots,N$ is the Laplacian spectrum of the weighted RPMG.

This interesting observation enables us to employ, for the analysis of the CL accuracy, results from spectral graph theory (e.g., [48]–[50]), where the properties of the Laplacian eigenvalues and their relations to the properties of graphs have been extensively studied. In (27), we observe that the second term, expressing the effects of the RPMG topology on the steady-state covariance, is a decreasing function of the eigenvalues of $\mathbf{C}_u$ (and thus, of the Laplacian eigenvalues $\lambda_{\mathcal{L}_k}$). Thus, to maximize the positioning accuracy, RPMG topologies that result in large Laplacian eigenvalues should be sought. Moreover, in [45], it is shown that the smallest eigenvalue of $\mathbf{C}_u$ defines the *time constant* of the transient behavior of the covariance matrix. In a scenario where the initial uncertainty of the robots is large, and fast convergence to steady state is necessary, selecting an RPMG topology that maximizes the smallest Laplacian eigenvalue can, thus, be a useful strategy. Since determining optimal RPMG topologies is not the primary focus of this paper, we will not expand further on this issue here. However, the development of algorithms for determining the optimal graph topology, given constraints on the number of measurements, is an interesting avenue for future research.

B. Upper Bound on Expected Steady-State Covariance

The results of the preceding section enable us to determine the *guaranteed accuracy* of CL for a team of robots with a given set of sensors, and a specified RPMG topology. The bounds determined in (26) and (27) hold for any scenario of the robots' motion, as long as the maximum distance between any pair of them remains smaller than ρ_o. However, it is the case for many practical scenarios that a better characterization of the robots' trajectories is known in advance. For example, we may be able to model the pose of the robots by a known probability distribution function (pdf) in their operational area. In this case, the covariance matrices $\mathbf{Q}(k+1)$ and $\mathbf{R}_{o_i}(k+1)$ [(5) and (14)] are functions of random variables, whose mean value can be determined. The availability of additional knowledge in the form of a prior distribution for the robots' poses can be used in order to attain a tighter upper bound on the *expected* covariance of the position estimates in CL.

Specifically, it can be shown [45] that the right-hand side of (20) is a concave function of the matrix

$$\begin{bmatrix} \mathbf{P}_k & \mathbf{0} \\ \mathbf{0} & \mathbf{R}_o(k+1) \end{bmatrix}.$$

This property enables us to employ Jensen's inequality [51] to prove, by induction, the following lemma [45].

Lemma 4: If $\bar{\mathbf{R}} = E\{\mathbf{R}_o(k+1)\}$ and $\bar{\mathbf{Q}} = E\{\mathbf{Q}(k+1)\}$ are the expected values of the measurement and system noise covariance matrices, respectively, then the solution to the following Riccati recursion:

$$\bar{\mathbf{P}}_{k+1} = \bar{\mathbf{P}}_k - \bar{\mathbf{P}}_k\mathbf{H}_o^T\left(\mathbf{H}_o\bar{\mathbf{P}}_k\mathbf{H}_o^T + \bar{\mathbf{R}}\right)^{-1}\mathbf{H}_o\bar{\mathbf{P}}_k + \bar{\mathbf{Q}} \quad (31)$$

with initial condition $\bar{\mathbf{P}}_0 = \mathbf{P}_0$, satisfies $\bar{\mathbf{P}}_k \succeq E\{\mathbf{P}_k\}$ for all $k \geq 0$.

In other words, evaluating the average values of the covariance matrices $\mathbf{R}_o(k+1)$ and $\mathbf{Q}(k+1)$ enables us to formulate a *constant coefficient* Riccati recursion, whose solution is an upper bound on the *expected* covariance of the position estimates in CL. Clearly, once the values $\bar{\mathbf{R}}$ and $\bar{\mathbf{Q}}$ have been determined, the derivations are analogous to the ones presented in the preceding section.

The average value of the system noise covariance matrix is easily computed by averaging over all values of orientation of the robots. Assuming a uniform distribution of the robots' orientation, from (4), we obtain

$$E\{Q_i(k+1,k+1)\} = \delta t^2\frac{\sigma_{V_i}^2 + \sigma_{\phi_i}^2 V_{m_i}^2}{2}I_2 = \bar{q}_i I_2 \quad (32)$$

and thus

$$\bar{\mathbf{Q}} = E\{\mathbf{Q}(k+1)\} = \mathbf{Diag}(\bar{q}_i I_2). \quad (33)$$

In order to evaluate the expected value of $\mathbf{R}_o(k+1)$, we assume that the positions of the robots are modeled by a uniform[3] pdf, inside a rectangular area of side α. Using the definition of $\boldsymbol{R}_{o_i}(k+1)$ in (14), it can be shown that the expected value of $\boldsymbol{R}_{o_i}(k+1)$ equals

$$\bar{\mathbf{R}}_i = \left(\sigma_{\rho_i}^2\frac{\alpha^2}{2} + \sigma_{\theta_i}^2\frac{\alpha^2}{6} + \sigma_{\phi_i}^2\frac{\alpha^2}{12}\right)I_{2M_i} + \sigma_{\phi_i}^2\frac{\alpha^2}{12}\mathbf{1}_{2M_i\times 2M_i}$$

and thus

$$\bar{\mathbf{R}} = \begin{bmatrix} \mathbf{Diag}(\bar{\mathbf{R}}_i) & \mathbf{0} \\ \mathbf{0} & \mathbf{Diag}\left(\mathbf{R}_{a_i}\right) \end{bmatrix}. \quad (34)$$

Using these results, upper bounds on the expected steady-state covariance of the position estimates in CL, for both the observable and unobservable case, can be derived. The solutions of the Riccati recursion in (31) for the two cases are completely analogous to those presented in Lemmas 2 and 3, with the sole difference that the quantities $\mathbf{Q}_u$ and $\mathbf{R}_u$ are replaced by $\bar{\mathbf{Q}}$ and $\bar{\mathbf{R}}$, respectively (and therefore, the matrix $\mathbf{C}_u$ is also replaced by $\bar{\mathbf{C}} = \bar{\mathbf{Q}}^{1/2}\mathbf{H}_o^T\bar{\mathbf{R}}^{-1}\mathbf{H}_o\bar{\mathbf{Q}}^{1/2}$).

Some interesting remarks can be made about the uncertainty increase rate in a robot team that has no access to absolute position information. The upper bound on the expected rate of increase is equal to $\bar{q}_T\delta t^{-1}$, where

$$\frac{1}{\bar{q}_T} = \sum_{i=1}^{N}\frac{1}{\bar{q}_i}. \quad (35)$$

We once again underline the fact that the maximum expected rate of uncertainty increase is *independent* of the initial uncertainty $\mathbf{P}_0$, the accuracy of the relative position measurements, and the topology of the RPMG. Moreover, we can compare this

[3]The uniform distribution was employed in the calculation of $\bar{\mathbf{R}}$, since it was deemed an appropriate model for the positions of the robots in the experiments presented in Section VI. However, the analysis holds for any given pdf.

value with the rate at which uncertainty increases when each robot localizes independently, using DR. In that case, the covariance matrix for all robots' estimates evolves in time according to (6), and therefore, the average rate of increase in uncertainty for robot i is

$$E\left\{\frac{1}{\delta t}\left(P_{i_{k+1}}-P_{i_k}\right)\right\}=E\left\{\frac{1}{\delta t}Q_i(k,k)\right\}=\frac{\bar{q}_i}{\delta t}I_2 \Rightarrow$$
$$E\left\{P_{i_{k+1}}\right\}=E\left\{P_{i_k}\right\}+\bar{q}_i I_2. \quad (36)$$

From the definition of $\bar{q}_T$ [cf. (35)], it becomes clear that it will be smaller than the smallest of the $\bar{q}_i$'s (notice that the definition of $\bar{q}_T$ is analogous to the expression for the total resistance of resistors in parallel). This implies that it suffices to equip only *one* robot in the team with proprioceptive sensors of high accuracy, in order to achieve a desired rate of uncertainty increase. *All* the robots of the group will experience a reduction in the rate at which their uncertainty increases and this improvement is more significant for robots with sensors of poor quality. Moreover, the maximum expected rate of uncertainty increase is *identical* for all robots of the team, regardless of the accuracy of each robot's odometry, and it decreases as the number of robots, N, increases.

Corollary 5: The maximum expected rate of positioning uncertainty increase of all the robots of a heterogeneous team performing CL is the *same*, equal to $\bar{q}_T\delta t^{-1}$, where

$$\frac{1}{\bar{q}_T}=\sum_{i=1}^{N}\frac{1}{\bar{q}_i}\geq\max\left(\frac{1}{\bar{q}_i}\right)\Rightarrow\bar{q}_T\leq\min\bar{q}_i. \quad (37)$$

This rate is *smaller* than the rate of uncertainty increase of the robot with the best DR performance, if it were to localize independently.

Before presenting the experimental and simulation results that corroborate the theoretical analysis, in the following section, we study some important properties of the derived upper bounds.

V. RPMG Reconfigurations

In the preceding analysis, it is assumed that the topology of the graph describing the relative position measurements between robots does not change. However, this may be difficult to implement in a realistic scenario. For example, due to the robots' motion or because of obstacles in the environment, some robots may not be able to measure their relative positions. Additionally, robot teams often need to allocate computational and communication resources to mission-specific tasks and this may force them to reduce the number of measurements they process for localization purposes. Consequently, it is of considerable interest to study the effects of changes in the topology of the RPMG on the localization accuracy of the team.

Consider the following scenario: At the initial stage of the deployment of a robotic team, the RPMG has a dense topology $\mathcal{T}_1$, e.g., the complete graph shown in Fig. 5(a), and retains this topology until some time instant t_1, when it assumes a sparser topology $\mathcal{T}_2$, e.g., the ring graph shown in Fig. 5(b). This sparse topology may even be an *empty graph*, i.e., the case in which the robots localize independently, based only on DR. Subsequent topology changes are assumed to occur at time instants t_i, $i=1\ldots n-1$, and finally, at time instant t_n, the RPMG returns to its initial, dense topology, $\mathcal{T}_1$. Assuming that the time intervals (t_{i-1},t_i) are of sufficient duration for the transient phenomena in the time evolution of uncertainty to subside, the following lemma, whose proof can be found in Appendix III, applies.

Lemma 6: After a sequence of RPMG reconfigurations and once the RPMG resumes its initial topology, the maximum expected positioning uncertainty of the robots at steady-state is *identical* to the one the robot team would have if no RPMG reconfigurations had taken place.

This implies that during time intervals when the RPMG topology is a sparse one, the "additional uncertainty" is introduced in directions of the state space that belong in the observable subspace. Thus, when the topology resumes its initial dense form, this additional uncertainty vanishes.

This is a significant result due to its important implications. Consider the scenario where the robots of a team, during a phase of their mission, are forced to receive and process a small number of measurements, or even resort to mere DR, due to communication or sensor failures, or because CPU and bandwidth resources are required by other tasks of higher priority. During this interval, a reduced amount of positioning information is available to the robots (sparse RPMG topology) and as a result the performance of CL will temporarily deteriorate. However, once the initial, dense RPMG topology is restored, the team's positioning performance will have sustained *no degradation*. Furthermore, Lemma 6 indicates that a dense topology for the RPMG during the initial phase of the deployment of a robot team has a long-term effect on the localization performance of the team. Specifically, if during the initial deployment, the robots leverage their communication and computational resources to support a dense RPMG, this will improve their positioning accuracy at the beginning of CL. Later on, and as the robots focus on mission-specific and other time-critical tasks, they will have to rely on sparser RPMGs as resources dictate. However, when at a subsequent time instant the RPMG resumes its initial, dense topology, the above lemma guarantees that the maximum expected uncertainty will be *identical* to the one that would arise if the dense RPMG topology was retained throughout the run of the robots.

VI. Experimental Results

A series of experiments were conducted for validating the preceding theoretical analysis. Our experimental setup is shown in Fig. 1(a). A team of four Pioneer I robots moves in a rectangular area, within which the positions of the robots are being tracked by an overhead camera. For this purpose, rectangular targets are mounted on top of the robots and the vision system is calibrated in order to provide measurements of the pose of the robots in a global coordinate frame. The standard deviation of the noise in these measurements is approximately 0.5° for orientation and 1 cm, along each axis, for position. The robots were commanded to move at a constant velocity of $V=0.1$ m/s while avoiding collision with the boundaries of the arena as well as with their teammates.

Although four identical robots were used, calibration of their odometric sensors showed that the accuracy of the wheel

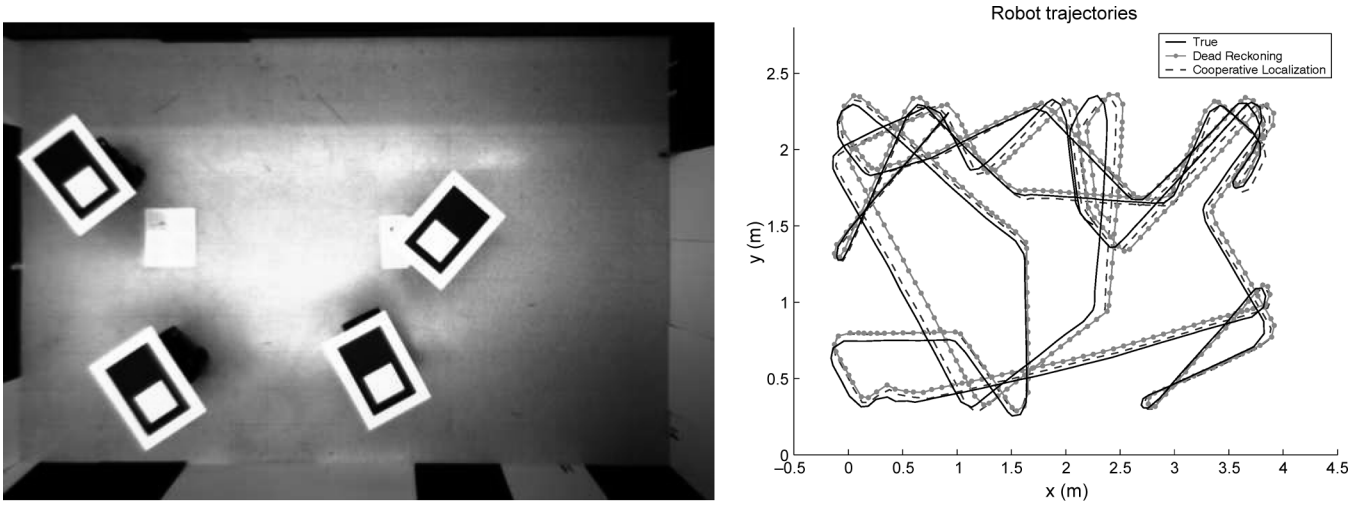

(a) (b)

Fig. 1. (a) Calibrated image of robots with targets mounted on top of them. (b) True and estimated trajectories for robot 1. For presentation clarity, only part of the trajectory, corresponding to the first 450 s, is plotted. The size of the arena is approximately 2.5×4.5 m.

encoder measurements is *not* identical for all robots. Specifically, the measurement errors are well-modeled as Gaussian zero-mean white noise processes and the standard deviation of the velocity measurements ranges from $\sigma_{V_{\min}} = 0.038V$, for the most accurate odometer to $\sigma_{V_{\max}} = 0.069V$, for the robot with the highest noise levels. Similarly, the standard deviations of the rotational velocity measurements have values between $\sigma_{\omega_{\min}} = 0.0078$ rad/s and $\sigma_{\omega_{\max}} = 0.02$ rad/s for the four robots. We observe that as a result of the variability of sensor characteristics, attributed to manufacturing imperfections, the experiments involve a heterogeneous robot team, although this had not been planned for. This shows the practical significance of raising the assumption of a homogeneous robot team, which had been imposed in previous work [12].

Each of the robots is equipped with a laser range finder, that is used for measuring absolute orientation. This is done by exploiting the perpendicularity of the surfaces surrounding the arena and employing a simple line-fitting technique. The standard deviation of the errors in the orientation measurements is approximately 0.5° for all robots.

Relative position measurements are produced synthetically using the differences in the positions of the robots, as these are recorded by the overhead camera, expressed in the measuring robot's coordinate frame, with the addition of noise. This facilitates the study of the effects of varying the accuracy of the relative position measurements and allows for control of the topology of the RPMG. For the experimental results shown in this section, a complete RPMG topology is formed and the relative position measurements (distance and bearing) are corrupted by zero-mean white Gaussian noise processes with standard deviation $\sigma_\rho = 0.05$ m and $\sigma_\theta = 0.0349$ rad. Position estimation was run offline and all measurements were downsampled to the rate of 1 Hz, so as to achieve synchronization.

In Fig. 1(b), the true trajectory (solid line) for one of the robots, as measured by the overhead camera, is compared with the trajectory estimated using DR (solid line with dots) and CL (dashed line). The significant improvement in positioning performance, resulting from the use of relative position information, is apparent and is demonstrated more clearly in Fig. 2, where the time evolution of the covariance is shown. Fig. 2(a) corresponds to the case in which the four robots localize independently, and compares the expected covariance values computed by (36) (dashed lines), with the covariance values computed by the filter (solid lines). On the other hand, Fig. 2(b) corresponds to the CL case and presents the covariance computed by the EKF (solid lines) as well as the theoretically derived upper bound for the expected covariance (dashed lines) and the upper bound for the worst-case covariance (dash-dotted lines). It is evident that the derived upper bound is indeed larger than the actual covariance of the position estimates. Moreover, we note that despite the fact that we deal with a heterogeneous team, the positioning uncertainty increases at the *same* rate for all robots. This rate is significantly smaller compared with that of the robot with the most accurate sensors localizing when relying on DR [in this case, Robot 2 as shown in Fig. 2(a)]. This observation agrees with the theoretical result of Corollary 5.

In Fig. 3, the errors in the position estimates of the robots are plotted and compared against the $\pm 3\sigma$ values of the position estimates' covariance. The solid lines represent the $\pm 3\sigma$ values associated with the covariance computed by the EKF, while the dashed ones represent the $\pm 3\sigma$ values computed using (36) for the case of DR, and the upper bound on the expected covariance for the case of CL. In these plots, the substantial improvement in positioning accuracy, achieved when the robots are recording and processing relative position measurements, is illustrated. However, the most important conclusion drawn from these figures is that the derived analytical expressions can be employed in order to accurately *predict* the localization performance of a robot team. The $\pm 3\sigma$ enveloping lines, evaluated using the derived analytical expressions, define a confidence region that closely describes the magnitude of the position errors. This justifies the use of the covariance matrix as a performance metric and demonstrates that for a robot team with known sensor noise characteristics, it is possible to characterize its positioning

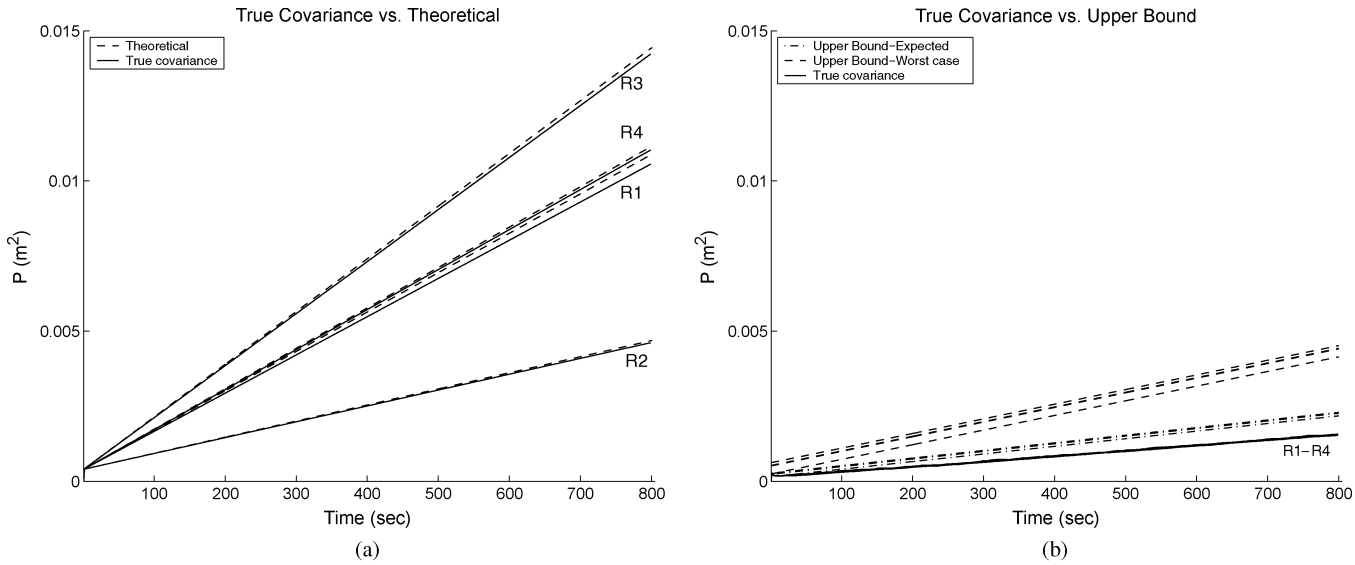

Fig. 2. Time evolution of the true covariance of the position estimates (solid bounding lines) and theoretically computed values (dashed black lines). (a) DR. (b) CL.

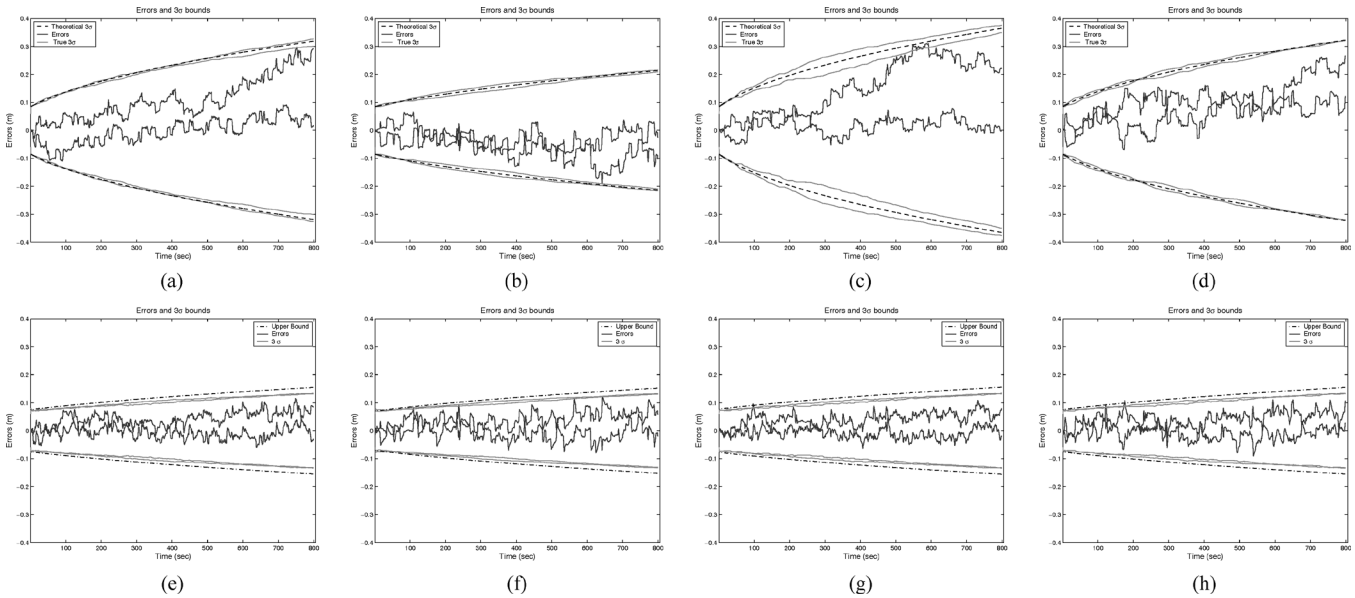

Fig. 3. Top row: Errors (solid blue lines) in the position estimates for the robots when they perform DR. Bottom row: Position errors during CL. The solid bounding lines represent the $\pm 3\sigma$ values of the actual covariance, computed by the EKF, while the dash–dotted bounding lines represent the $\pm 3\sigma$ values computed employing the theoretical upper bound for the expected covariance. (a) Robot 1-DR. (b) Robot 2-DR. (c) Robot 3-DR. (d) Robot 4-DR. (e) Robot 1-CL. (f) Robot 2-CL. (g) Robot 3-CL. (h) Robot 4-CL.

accuracy, without having to resort to extensive simulations, or experimentation.

VII. Simulation Results

In this section, we present simulation results that demonstrate the effect of RPMG reconfigurations and corroborate the corresponding theoretical analysis. In order to isolate the effects of different RPMG topologies, a homogeneous team comprising nine robots is considered in these simulations. Note, however, that as the previous section demonstrates, homogeneity is not a prerequisite of our approach. The robots are restricted to move in an area of radius $r = 20$ m, and their velocity is assumed to be constant, equal to $V_i = 0.25$ m/s. The orientation of the robots, while they move, changes randomly using samples drawn from a uniform distribution of width 20° about 0°.

The parameters of the noise that corrupts the proprioceptive measurements of the simulated robots are identical to those measured on a iRobot PackBot robot ($\sigma_V = 0.0125$ m/s, $\sigma_\omega = 0.0384$ rad/s). The absolute orientation of each robot was measured by a simulated compass with $\sigma_\phi = 0.0524$ rad. The robot tracker sensor returned range and bearing measurements corrupted by zero-mean white noise with $\sigma_\rho = 0.01$ m and $\sigma_\theta = 0.0349$ rad. The above values are compatible with noise parameters observed in laboratory experiments [17]. All measurements were available at 1 Hz.

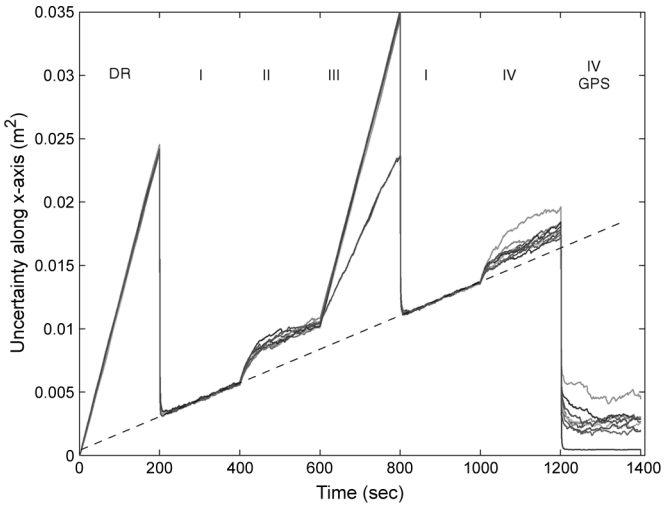

Fig. 4. Uncertainty evolution for a RPMG with changing topology. The dashed straight line has been superimposed on the figure to facilitate the comparison between the values of the covariances for different topologies of the RMPG.

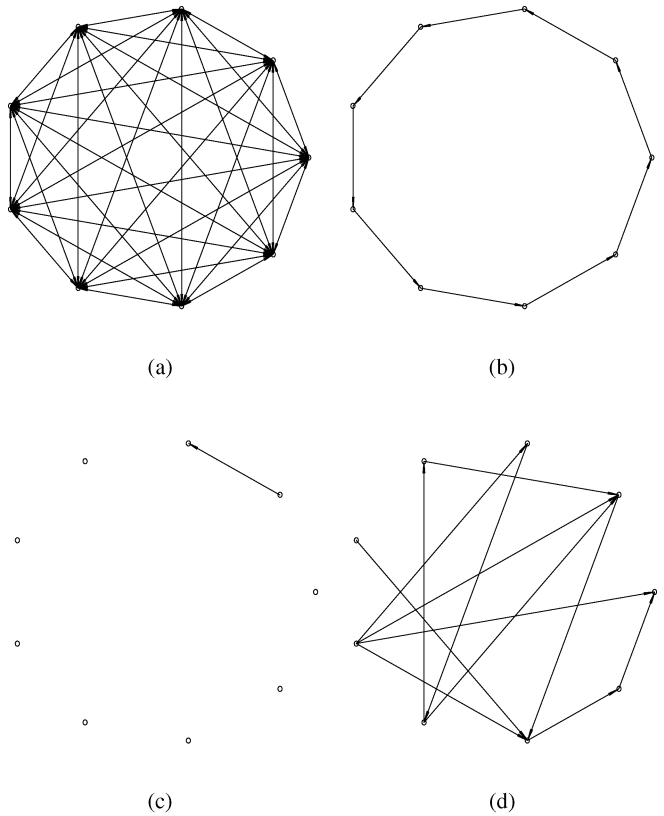

Fig. 5. Four different RPMG topologies considered in the simulations. Each arrow represents a relative position measurement, with the robot (node) where the arrow starts being the observing robot. (a) Graph I.(b) Graph II. (c) Graph III. (d) Graph IV.

In Fig. 4, the time evolution of the positioning uncertainty of the robot team is shown. Initially, up to $t = 200$ s, the robots do not record any relative position measurements and propagate their position estimates using DR. At $t = 200$ s, the robots start receiving relative position measurements and the topology of the RPMG becomes a complete one [Fig. 5(a)]. The significant reduction in the rate of uncertainty increase, achieved by using relative positioning information, is demonstrated in this transition. At $t = 400$ s, the RPMG assumes a ring topology [Fig. 5(b)]. We note that the uncertainty undergoes a transient phase, during which it increases at a higher rate and then, once steady state is reached, the rate of increase is *identical* to the rate associated with the complete graph. This corroborates the result of (27) and shows that the dominant factor in determining the rate of localization uncertainty increase is the quality of the proprioceptive and orientation sensors of the robots.

At $t = 600$ s, a hypothetical failure of the communication network occurs, and in the time interval between 600–800 s, only two robots are able to measure their relative positions [Fig. 5(c)]. This case can be viewed as a degenerate one, where the seven robots localize based solely on DR, while the other two robots form a smaller team. As expected, the rate of uncertainty increase is higher when the team consists of only two robots, instead of nine, but lower when compared with DR.

At $t = 800$ s, the RPMG resumes the complete graph topology [Fig. 5(a)]. It is evident that the average uncertainty in the position estimates during the time intervals (200, 400) and (800, 1000) s is described by the *same* linear function of time. This occurs despite the prior two reconfigurations of the topology of the RPMG that occurred at $t = 400$ s and $t = 600$ s. This result is in accordance with the theoretical analysis of Section V.

At $t = 1000$ s, the RPMG assumes a noncanonical topology, i.e., random graph [Fig. 5(d)]. This scenario is perhaps the most important one for real applications, since robots will usually measure the relative positions of neighboring robots that are within their field of view. Due to the robots' motion, the topology of the RPMG can change randomly. We observe that the positioning uncertainty increases at a rate identical to that of Phases I and II of the graph's topology, as predicted by our theoretical analysis. It is also apparent that the uncertainty for each robot converges to a set of lines with the same slope (rate of uncertainty increase), but different constant offset. This is due to the effect of the different degree of connectivity in the RPMG of each robot. Connection-rich robots have direct access to positioning information from more robots and thus, attain lower positioning uncertainty.

Finally, at $t = 1200$ s, only one of the robots starts receiving GPS measurements while the RPMG retains the topology of Fig. 5(d). The GPS measurements are corrupted by noise with a standard deviation of $\sigma_{\rm GPS} = 0.05$ m in each axis. It is evident that the availability of absolute position measurements to *any* robot drastically reduces the localization uncertainty for *all* the robots in the group. Furthermore, the system becomes observable and the uncertainty is bounded for all the members of the team. As in the previous phase, the uncertainty for the position of each robot converges to a value (constant in this case) that depends on its degree of connectivity.

VIII. Conclusion

This paper presents an in-depth study of the localization performance of heterogeneous robotic teams with arbitrary and potentially dynamic RPMG topologies. A *functional relation* has been established between the maximum expected positioning uncertainty during CL and design parameters such as: 1) the

size of the robot group; 2) the accuracy of the robots' sensors; and 3) the topology of the RPMG. When the precision of the position estimates of a team is required to meet specifications imposed by a certain task, the derived expressions can be employed to facilitate the selection of the required parameters of the robot group. The presented theoretical analysis allows the prediction of the magnitude of the CL position errors when the topology of the RPMG changes or when the size of the robot team varies over time (e.g., when robots are located out of measurement/communication range or they fail temporarily or permanently). Furthermore, the case in which absolute positioning information (e.g., from a GPS receiver, or from a precompiled map) is available to at least one of the team members, is naturally incorporated in this framework. Thus, this work offers a powerful tool that allows for determining the positioning capabilities of a multi-robot system early on in the design stage, without the need to resort to extensive simulations, or time-consuming experimentation.

Significant properties of the time evolution of the positioning uncertainty have been presented. It was shown that even if *one* robot has access to absolute position measurements, the positioning uncertainty of *all* the robots in the group remains bounded and converges to a constant value. In contrast, for a robot team whose members only register relative position measurements, Lemma 3 maintains that at steady-state, the increase rate of the maximum uncertainty is *independent* of both the accuracy of the robot tracker device and the topology of the RPMG. Aside from the number of robots comprising the team, the single most important factor that determines the uncertainty of the position estimates is the accuracy of the proprioceptive sensors and orientation estimates of the robots. In the particular case of a heterogeneous robot group, the localization accuracy of the robot equipped with the *most precise* sensors is the one that has the greatest impact on the overall accuracy.

These observations are of great practical importance since they ensure that for a robot group of certain size, the *number* of relative position measurements affects only the constant term of the covariance while the rate of uncertainty increase remains the same. Furthermore, it was shown that if the robots are forced to temporarily reduce the number of recorded relative position measurements (due to external factors such as visibility constraints, or because of resource allocation to time-critical tasks), then when the RPMG resumes its prior topology, *no loss of localization performance* is inflicted. These properties can be extremely useful when designing robotic teams for specific applications, or when considering task planning and/or motion strategy for robot groups operating in adverse environments.

An interesting direction for future research is the study of the underlying relationship between the CL performance and the Laplacian eigenvalues of the RPMG. Initial results indicate that employing concepts from Spectral Graph Theory can facilitate the description of the properties of the time evolution of positioning uncertainty, in terms of the characteristics of the RPMG. This analysis is especially important for robotic teams of large size, in which the asymptotic properties of the Laplacian eigenvalues of the graph become dominant. We are currently investigating the existence of optimal graph topologies that, given constraints on the available resources, provide optimal positioning performance [44]. To this end, the effect of graph characteristics, such as diameter, average path length, and clustering coefficient, on the positioning performance of the robotic team are examined.

APPENDIX I

In this appendix, we derive an upper bound for $\boldsymbol{R}_{o_i}(k)$, by considering each of the terms in (14) independently. The term that expresses the effect of noise in the range measurements is

$$R_1(k) = \sigma_{\rho_i}^2 I_{2M_i} - D_i \mathrm{diag}\left(\frac{\sigma_{\rho_i}^2}{\hat{\rho}_{ij}^2(k)}\right) D_i^T \preceq \sigma_{\rho_i}^2 I_{2M_i} \quad (38)$$

where the matrix inequality follows from the fact that the negative term in the expression for $R_1(k)$ is a positive semi-definite matrix. The covariance term due to the noise in the bearing measurement is

$$\begin{aligned} R_2(k) &= \sigma_{\theta_i}^2 D_i D_i^T \\ &= \sigma_{\theta_i}^2 \mathbf{Diag}\left(\hat{\rho}_{ij}^2 \begin{bmatrix} \sin^2(\hat{\theta}_{ij}) & \sin(\theta_{ij})\cos(\hat{\theta}_{ij}) \\ \sin(\hat{\theta}_{ij})\cos(\hat{\theta}_{ij}) & \cos^2(\hat{\theta}_{ij}) \end{bmatrix}\right) \\ &\preceq \sigma_{\theta_i}^2 \mathbf{Diag}\left(\hat{\rho}_{ij}^2 I_2\right) \\ &\preceq \sigma_{\theta_i}^2 \rho_o^2 I_{2M_i} \end{aligned} \quad (39)$$

where ρ_o is the maximum possible distance between any two robots. Finally, the covariance term expressing the error in the orientation of the measuring robot is

$$\begin{aligned} R_3(k) &= \sigma_{\phi_i}^2 D_i \mathbf{1}_{M_i \times M_i} D_i^T \\ &\preceq \sigma_{\phi_i}^2 D_i \left(M_i I_{M_i}\right) D_i^T = M_i \sigma_{\phi_i}^2 D_i D_i^T. \end{aligned}$$

By derivations analogous to those employed to yield an upper bound for $R_2(k)$, it can be shown that

$$R_3(k) \preceq M_i \sigma_{\phi_i}^2 \rho_o^2 I_{2M_i}. \quad (40)$$

Combining this result with those of (38) and (39), we can write $\boldsymbol{R}_{o_i}(k) = R_1(k) + R_2(k) + R_3(k) \preceq r_i I_{2M_i}$, where

$$r_i = \sigma_{\rho_i}^2 + M_i \sigma_{\phi_i}^2 \rho_o^2 + \sigma_{\theta_i}^2 \rho_o^2. \quad (41)$$

APPENDIX II

In this appendix, we show how to derive the steady-state solution of the Riccati recursion in (25). We denote the SVD of matrix $\mathbf{C}_u$ as $\mathbf{C}_u = \mathbf{U}\mathrm{diag}(\lambda_i)\mathbf{U}^T = \mathbf{U}\Lambda\mathbf{U}^T$, and defining $\mathbf{P}_{nn_k} = \mathbf{U}^T \mathbf{P}_{n_k} \mathbf{U}$ yields the recursion

$$\mathbf{P}_{nn_{k+1}} = \mathbf{P}_{nn_k} \left(I_{2N} + \Lambda \mathbf{P}_{nn_k}\right)^{-1} + I_{2N}. \quad (42)$$

When the system is observable, at steady-state, we have $\mathbf{P}_{nn_{k+1}} = \mathbf{P}_{nn_k} = \mathbf{P}_{nn_\infty}$, and we thus need to solve the matrix equation

$$\mathbf{P}_{nn_\infty} = \mathbf{P}_{nn_\infty} \left(I_{2N} + \Lambda \mathbf{P}_{nn_\infty}\right)^{-1} + I_{2N}.$$

In this expression, all the diagonal elements of Λ are positive, since $\mathbf{C}_u$ is a positive definite matrix [45]. Assuming a diagonal form for $\mathbf{P}_{nn_\infty}$, we can easily derive the solution

$$\mathbf{P}_{nn_\infty} = \mathrm{diag}\left(\frac{1}{2} + \sqrt{\frac{1}{4} + \frac{1}{\lambda_i}}\right).$$

However, the fact that we are dealing with an observable system, means that the asymptotic solution to the Riccati recursion is unique [52]. Thus, the above derived solution is unique, and from it, the expression in (26) follows directly from the relation $\mathbf{P}_k^u = \mathbf{Q}_u^{1/2}\mathbf{U}\mathbf{P}_{nn_k}\mathbf{U}^T\mathbf{Q}_u^{1/2}$.

When none of the robots has access to absolute position measurements, the system is unobservable, and the asymptotic solution to the Riccati recursion in (25) [or, equivalently, in (42)] is not as straightforward, since the solution now depends on the initial value of the covariance matrix. When the system is unobservable, matrix $\mathbf{C}_u$ is of rank $2N-2$, and therefore, two of its singular values equal zero [45].

We first address the case in which the initial covariance matrix is zero. We observe that the right-hand side of (42) is a diagonal matrix in this case, and by a simple induction argument, we can show that the solution to this recursion retains a diagonal form for all $k \geq 0$. Addressing each of the diagonal elements individually, we observe that for the first $2N-2$ elements, which correspond to the nonzero singular values, we obtain the equations

$$\mathbf{P}_{nn_{k+1}}(i,i) = \mathbf{P}_{nn_k}(i,i)\left(1 + \lambda_i \mathbf{P}_{nn_k}(i,i)\right)^{-1} + 1$$

while for the last two elements, we obtain

$$\mathbf{P}_{nn_{k+1}}(i,i) = \mathbf{P}_{nn_k}(i,i) + 1.$$

Therefore, the asymptotic solution for $\mathbf{P}_{nn_k}$ is given by

$$\mathbf{P}_{nn_k} = \begin{bmatrix} \mathrm{diag}_\xi\left(\frac{1}{2} + \sqrt{\frac{1}{4} + \frac{1}{\lambda_i}}\right) & \mathbf{0}_{(2N-2)\times 2} \\ \mathbf{0}_{2\times(2N-2)} & kI_2 \end{bmatrix}. \quad (43)$$

Employing the relation $\mathbf{P}_k^u = \mathbf{Q}_u^{1/2}\mathbf{U}\mathbf{P}_{nn_k}\mathbf{U}^T\mathbf{Q}_u^{1/2}$ and the last result, we obtain the first two terms in (27). For this derivation, the basis vectors of the nullspace of the matrix $\mathbf{C}_u$ are needed. Recall that in Section III-B, the nullspace of $\mathbf{H}_o$ was shown to be spanned by the column vectors of $V = \mathbf{1}_{N\times 1} \otimes I_2$, and thus, we can easily see that a basis of the nullspace of $\mathbf{C}_u = \mathbf{Q}_u^{1/2}\mathbf{H}_o^T\mathbf{R}_u^{-1}\mathbf{H}_o\mathbf{Q}_u^{1/2}$ is defined by the columns of $V_\mathbf{C} = g^{-1}\mathbf{Q}_u^{-1/2}V$, where g is a normalizing factor to ensure unit norm. Using this result, the derivation of the first two terms in (27) now merely involves algebraic manipulation.

In order to derive the last term of that equation, which depends on the initial uncertainty, we first define the matrix $\tilde{\mathbf{P}}_k = \mathbf{P}_{n_k} - kV_\mathbf{C}V_\mathbf{C}^T$. This matrix has the property that it asymptotically approaches a constant value, depending on the initial covariance matrix. Substitution in (25) and simple algebraic manipulation results in the recursion

$$\tilde{\mathbf{P}}_{k+1} = \tilde{\mathbf{P}}_k\left(I_{2N} + \mathbf{C}_u\tilde{\mathbf{P}}_k\right)^{-1} + \mathbf{U}\begin{bmatrix} I_\xi & \mathbf{0}_{\xi\times 2} \\ \mathbf{0}_{2\times\xi} & \mathbf{0}_{2\times 2} \end{bmatrix}\mathbf{U}^T \quad (44)$$

where $\xi = 2N-2$ is the number of nonzero eigenvalues of $\mathbf{C}_u$. The solution of this recursion is derived employing the following lemma (adapted from [52]).

Lemma 7: Suppose $\tilde{\mathbf{P}}_k^{(0)}$ is the solution to the Riccati recursion in (44) with zero initial condition. Then the solution to this recursion when the initial covariance matrix is an arbitrary positive semidefinite matrix $\tilde{\mathbf{P}}_0$ is defined by the relation

$$\tilde{\mathbf{P}}_{k+1} - \tilde{\mathbf{P}}_{k+1}^{(0)} = \Phi_p^{(0)}(k+1)\left(I_{2N} + \tilde{\mathbf{P}}_0\mathbf{J}_{k+1}\right)^{-1}\tilde{\mathbf{P}}_0\Phi_p^{(0)}(k+1)^T$$

where

$$\Phi_p^{(0)}(k+1) = \left(I_{2N} - \tilde{\mathbf{P}}\mathbf{H}_o^T\left(\mathbf{H}_o\tilde{\mathbf{P}}\mathbf{H}_o^T + \mathbf{R}_u\right)^{-1}\mathbf{H}_o\right)^{k+1} \times \left(I_{2N} + \tilde{\mathbf{P}}\mathbf{J}_{k+1}\right).$$

In these expressions, $\tilde{\mathbf{P}}$ is any solution to the discrete algebraic Riccati equation (DARE)

$$\tilde{\mathbf{P}} = \tilde{\mathbf{P}}\left(I_{2N} + \mathbf{C}_u\tilde{\mathbf{P}}\right)^{-1} + \mathbf{U}\begin{bmatrix} I_\xi & \mathbf{0}_{\xi\times 2} \\ \mathbf{0}_{2\times\xi} & \mathbf{0}_{2\times 2} \end{bmatrix}\mathbf{U}^T$$

and $\mathbf{J}_k$ denotes the solution to the *dual* Riccati recursion with zero initial condition

$$\mathbf{J}_{k+1} = \mathbf{J}_k + \mathbf{C}_u - \mathbf{J}_k\mathbf{U}\begin{bmatrix} I_\xi & \mathbf{0}_{\xi\times 2} \\ \mathbf{0}_{2\times\xi} & \mathbf{0}_{2\times 2} \end{bmatrix}\mathbf{U}^T\mathbf{J}_k.$$

We note that the zero-initial condition solution to (44) is straightforward to derive from (43) and the definition of $\tilde{\mathbf{P}}_k$. Additionally it is easy to show that this solution also constitutes a solution to the DARE. The detailed derivation of the final expression is quite lengthy, and cannot be included here due to limited space. The interested reader is referred to [45] for a thorough description of the intermediate steps.

APPENDIX III

Here, we prove Lemma 6. Due to space limitations, we provide a proof only for the scenario in which the sequence of reconfigurations involves exactly one intermediate topology, during which the RPMG is an empty graph. A generalization to the case of any sequence of reconfigurations, involving arbitrary RPMG topologies, is straightforward and is presented in [45].

The following proof is for the upper bound on the expected uncertainty, but a similar result holds for the worst-case bounds on the covariance. For this derivation, we employ (27) where we have substituted the quantities $\mathbf{Q}_u$ and $\mathbf{C}_u$ by $\bar{\mathbf{Q}}$ and $\bar{\mathbf{C}}$, respectively. It can be shown [45] that (27) can be written, in terms of the normalized covariance matrix, $\bar{\mathbf{P}}_n(k) = \bar{\mathbf{Q}}^{-1/2}\bar{\mathbf{P}}(k)\bar{\mathbf{Q}}^{-1/2}$, as

$$\bar{\mathbf{P}}_n(k) = \bar{\mathbf{U}}\begin{bmatrix} \mathrm{diag}_\xi\left(f(\bar{\lambda}_i)\right) & \mathbf{0}_{\xi\times 2} \\ \mathbf{0}_{2\times\xi} & kI_2 + \Psi \end{bmatrix}\bar{\mathbf{U}}^T \quad (45)$$

where $\bar{\lambda}_i$, $i = 1\ldots\xi$ are the nonzero singular values of $\bar{\mathbf{C}}$

$$f(\bar{\lambda}_i) = \frac{1}{2} + \sqrt{\frac{1}{4} + \frac{1}{\bar{\lambda}_i}}$$

and Ψ is a 2×2 matrix that encapsulates the effect of the initial uncertainty

$$\Psi = V^T \left(I_{2N} + \bar{\mathbf{P}}_n(0) h(\bar{\mathbf{C}})\right)^{-1} \bar{\mathbf{P}}_n(0) V. \tag{46}$$

In the last expression, $\mathbf{P}_n(0)$ is the normalized covariance at time $t_0 = 0$, and V is the $2N \times 2$ matrix comprising the singular vectors of $\bar{\mathbf{C}}$ corresponding to the zero singular values. The RPMG has the topology $\mathcal{T}_A$ for the time interval (t_0, t_1). The normalized covariance matrix at time t_1 is given by

$$\bar{\mathbf{P}}_n(t_1) = \bar{\mathbf{U}}_A \begin{bmatrix} \mathrm{diag}_\xi \left(f(\bar{\lambda}_i)\right) & \mathbf{0}_{\xi\times2} \\ \mathbf{0}_{2\times\xi} & t_1 I_2 + \Psi_A \end{bmatrix} \bar{\mathbf{U}}_A^T \tag{47}$$

where $\Psi_A = V^T(I_{2N} + \bar{\mathbf{P}}_n(0)h(\bar{\mathbf{C}}_A))^{-1}\bar{\mathbf{P}}_n(0)$. In these expressions, the subscript A has been appended to quantities that depend on the topology $\mathcal{T}_A$. In [45], it is shown that V is *independent* of the RPMG topology and thus, no subscript is necessary to identify it. Assuming that during the time interval (t_1, t_2) the robots perform DR, then the average rate of covariance increase during this time interval is equal to $\bar{\mathbf{Q}}$ [cf. (36)], and it is easy to show that at time t_2 the normalized covariance is given by:

$$\bar{\mathbf{P}}_n(t_2) = \bar{\mathbf{U}}_A \begin{bmatrix} \mathrm{diag}_\xi \left(f(\bar{\lambda}_{Ai})\right) + \Delta t_{12} I_\xi & \mathbf{0}_{\xi\times2} \\ \mathbf{0}_{2\times\xi} & t_2 I_2 + \Psi_A \end{bmatrix} \bar{\mathbf{U}}_A^T \tag{48}$$

where $\Delta t_{12} = t_2 - t_1$. In order to compute [through (45) and (46)] an upper bound on the uncertainty during Phase 3, when the RPMG resumes topology $\mathcal{T}_A$, the *exact* value of the covariance at time t_2 is needed. However, since we seek an upper bound for the covariance, we can use the fact that Ψ is a matrix-increasing function in the argument $\bar{\mathbf{P}}_n$, i.e., [45]

$$\bar{\mathbf{P}}'_n \succeq \bar{\mathbf{P}}_n \Rightarrow \Psi' \succeq \Psi. \tag{49}$$

Consequently, since (48) describes an upper bound on $\mathbf{Q}^{-1/2} E\{\mathbf{P}(t_2)\} \mathbf{Q}^{-1/2}$, the following expression is an upper bound on the normalized covariance at time $t > t_2$ (at steady-state):

$$\bar{\mathbf{P}}'_{n_A}(k) = \bar{\mathbf{U}}_A \begin{bmatrix} \mathrm{diag}_\xi \left(f(\bar{\lambda}_{Ai})\right) & \mathbf{0}_{\xi\times2} \\ \mathbf{0}_{2\times\xi} & (t - t_2) I_2 + \Psi'_A \end{bmatrix} \bar{\mathbf{U}}_A^T$$

where

$$\Psi'_A = V^T \left(I_{2N} + \bar{\mathbf{P}}_n(t_2) h(\bar{\mathbf{C}}_A)\right)^{-1} \bar{\mathbf{P}}_n(t_2) V$$

Substitution from (48) into the last expression and simple algebraic manipulation with the use of the matrix inversion lemma [45] yields

$$\Psi'_A = \Psi_A + t_2 I_2. \tag{50}$$

Thus

$$\bar{\mathbf{P}}'_{n_A}(k) = \bar{\mathbf{U}}_A \begin{bmatrix} \mathrm{diag}_\xi \left(f(\bar{\lambda}_{Ai})\right) & \mathbf{0}_{\xi\times2} \\ \mathbf{0}_{2\times\xi} & t I_2 + \Psi_A \end{bmatrix} \bar{\mathbf{U}}_A^T. \tag{51}$$

Clearly, the maximum expected steady-state covariance during Phase 3 is identical to the maximum expected covariance that would result from direct use of (47), i.e., *if no RPMG reconfigurations* had taken place.

ACKNOWLEDGMENT

The authors would like to thank the reviewers for their numerous constructive suggestions that greatly helped improve the quality of the manuscript.

REFERENCES

[1] W. Burgard, D. Fox, M. Moors, R. Simmons, and S. Thrun, "Collaborative multi-robot exploration," in *Proc. IEEE Int. Conf. Robot. Autom.*, San Francisco, CA, Apr. 2000, pp. 476–481.

[2] I. M. Rekleitis, G. Dudek, and E. Milios, "Multi-robot collaboration for robust exploration," *Ann. Math. Artif. Intell.*, vol. 31, no. 1–4, pp. 7–40, 2001.

[3] A. Yamashita, M. Fukuchi, J. Ota, T. Arai, and H. Asama, "Motion planning for cooperative transportation of a large object by multiple mobile robots in a 3D environment," in *Proc. IEEE Int. Conf. Robot. Autom.*, San Francisco, CA, Apr. 2000, pp. 3144–3151.

[4] T. L. Huntsberger, A. Trebi-Ollennu, H. Aghazarian, P. S. Schenker, P. Pirjanian, and H. D. Nayar, "Distributed control of multi-robot systems engaged in tightly coupled tasks," *Auton. Robots*, vol. 17, no. 1, pp. 79–92, Jul. 2004.

[5] J. Wawerla, G. S. Sukhatme, and M. J. Mataric, "Collective construction with multiple robots," in *Proc. IEEE/RSJ Int. Conf. Robot. Intell. Syst.*, Lausanne, Switzerland, Sep.–Oct. 2002, pp. 2696–2701.

[6] C. A. C. Parker, H. Zhang, and C. R. Kube, "Blind bulldozing: Multiple robot nest construction," in *Proc. IEEE/RSJ Int. Conf. Robot. Intell. Syst.*, Las Vegas, NV, Oct. 2003, pp. 2010–2015.

[7] R. Kurazume, S. Nagata, and S. Hirose, "Cooperative positioning with multiple robots," in *Proc. IEEE Int. Conf. Robot. Autom.*, Los Alamitos, CA, May 1994, pp. 1250–1257.

[8] I. M. Rekleitis, G. Dudek, and E. Milios, "Multi-robot exploration of an unknown environment, efficiently reducing the odometry error," in *Proc. 15th Int. Joint Conf. Artif. Intell.*, Nagoya, Japan, Aug. 1997, pp. 1340–1345.

[9] S. I. Roumeliotis and G. A. Bekey, "Collective localization: A distributed Kalman filter approach to localization of groups of mobile robots," in *Proc. IEEE Int. Conf. Robot. Autom.*, San Francisco, CA, Apr. 2000, pp. 2958–2965.

[10] T. Arai, E. Pagello, and L. E. Parker, "Editorial: Advances in multirobot systems," *IEEE Trans. Robot. Autom.*, vol. 18, no. 5, pp. 655–661, Oct. 2002.

[11] S. I. Roumeliotis and I. M. Rekleitis, "Analysis of multirobot localization uncertainty propagation," in *Proc. IEEE/RSJ Int. Conf. Robot. Intell. Syst.*, Las Vegas, NV, Oct. 2003, pp. 1763–1770.

[12] ——, "Propagation of uncertainty in cooperative multirobot localization: Analysis and experimental results," *Auton. Robots*, vol. 17, no. 1, pp. 41–54, Jul. 2004.

[13] R. Kurazume, S. Hirose, S. Nagata, and N. Sashida, "Study on cooperative positioning system (basic principle and measurement experiment)," in *Proc. IEEE Int. Conf. Robot. Autom.*, Minneapolis, MN, Apr. 1996, pp. 1421–1426.

[14] R. Kurazume and S. Hirose, "Study on cooperative positioning system: Optimum moving strategies for CPS-III," in *Proc. IEEE Int. Conf. Robot. Autom.*, Leuven, Belgium, May 1998, pp. 2896–2903.

[15] ——, "An experimental study of a cooperative positioning system," *Auton. Robots*, vol. 8, no. 1, pp. 43–52, Jan. 2000.

[16] R. Grabowski, L. E. Navarro-Serment, C. J. J. Paredis, and P. K. Khosla, "Heterogeneous teams of modular robots for mapping and exploration," *Auton. Robots*, vol. 8, no. 3, pp. 293–308, 2000.

[17] I. M. Rekleitis, G. Dudek, and E. Milios, "Probabilistic cooperative localization and mapping in practice," in *Proc. IEEE Int. Conf. Robot. Autom.*, Taipei, Taiwan, R.O.C., Sep. 2003, pp. 1907–1912.
[18] A. Rynn, W. A. Malik, and S. Lee, "Sensor-based localization for multiple mobile robots using virtual links," in *Proc. IEEE/RSJ Int. Conf. Robot. Intell. Syst.*, Las Vegas, NV, Oct. 2003, pp. 1771–1776.
[19] A. I. Mourikis and S. I. Roumeliotis, "Performance bounds for cooperative simultaneous localization and mapping (C-SLAM)," in *Proc. Robot. Sci. Syst. Conf.*, Cambridge, MA, Jun. 2005, pp. 281–288.
[20] D. Fox, W. Burgard, H. Kruppa, and S. Thrun, "Collaborative multirobot localization," in *Proc. 23rd Annu. German Conf. Artif. Intell.*, Bonn, Germany, Sep. 1999, pp. 255–266.
[21] ——, "A probabilistic approach to collaborative multi-robot localization," *Auton. Robots*, vol. 8, no. 3, pp. 325–344, Jun. 2000, Special Issue on Heterogeneous Multirobot Syst..
[22] S. Thrun, D. Fox, and W. Burgard, "Monte Carlo localization with mixture proposal distribution," in *Proc. AAAI Nat. Conf. Artif. Intell.*, Austin, TX, 2000, pp. 859–865.
[23] S. I. Roumeliotis, "Distributed multi-robot localization," Calif. Inst. Technol., Pasadena, 2002 [Online]. Available: http://robotics.caltech.edu/~stergios/tech_reports/tr_collective.pdf, Tech. Rep.
[24] A. Howard, M. J. Mataric, and G. Sukhatme, "Putting the 'i' in 'team': An ego-centric approach to cooperative localization," in *Proc. IEEE Int. Conf. Robot. Autom.*, Taipei, Taiwan, R.O.C., Sep. 2003, pp. 868–874.
[25] A. Howard, M. J. Mataric, and G. S. Sukhatme, "Localization for mobile robot teams using maximum likelihood estimation," in *Proc. IEEE/RSJ Int. Conf. Robot. Intell. Syst.*, Lausanne, Switzerland, Sep.–Oct. 2002, pp. 434–459.
[26] F. Dellaert, F. Alegre, and E. B. Martinson, "Intrinsic localization and mapping with 2 applications: Diffusion mapping and Marco Polo localization," in *Proc. IEEE Int. Conf. Robot. Autom.*, Taipei, Taiwan, R.O.C., Sep. 2003, pp. 2344–2349.
[27] A. C. Sanderson, "A distributed algorithm for cooperative navigation among multiple mobile robots," *Adv. Robot.*, vol. 12, no. 4, pp. 335–349, 1998.
[28] S. I. Roumeliotis and G. A. Bekey, "Distributed multirobot localization," *IEEE Trans. Robot. Autom.*, vol. 18, no. 5, pp. 781–795, Oct. 2002.
[29] I. M. Rekleitis, G. Dudek, and E. Milios, "Multi-robot cooperative localization: A study of trade-offs between efficiency and accuracy," in *Proc. IEEE/RSJ Int. Conf. Robot. Intell. Syst.*, Lausanne, Switzerland, Sep.–Oct. 2002, pp. 2690–2695.
[30] N. Trawny, "Optimized motion strategies for cooperative localization of mobile robots," M.S. thesis, Dept. Comput. Sci. Elect. Eng., Univ. Stuttgart, Stuttgart, Germany, 2003.
[31] I. M. Rekleitis and S. I. Roumeliotis, "Analytical expressions for positioning uncertainty propagation in networks of robots," in *Proc. 11th IEEE Mediterranean Conf. Control, Autom.*, Rhodes, Greece, Jun. 2003.
[32] A. I. Mourikis and S. I. Roumeliotis, "Analysis of positioning uncertainty in reconfigurable networks of heterogeneous mobile robots," in *Proc. IEEE Int. Conf. Robot. Autom.*, New Orleans, LA, Apr.–May 2004, pp. 572–579.
[33] A. Georgiev and P. K. Allen, "Localization methods for a mobile robot in urban environments," *IEEE Trans. Robot.*, vol. 20, no. 5, pp. 851–864, Oct. 2004.
[34] T. Duckett, S. Marsland, and J. Shapiro, "Simultaneous localization and mapping—A new algorithm for a compass-equipped mobile robot," presented at the IJCAI Workshop on Reasoning With Uncertainty in Robotics, Seattle, WA, Aug. 2001.
[35] R. Volpe, "Mars rover navigation results using sun sensor heading determination," in *Proc. IEEE/RSJ Int. Conf. Robot. Intell. Syst.*, Kyingju, Korea, Oct. 1999, pp. 467–469.
[36] A. Georgiev and P. K. Allen, "Design and analysis of a sun sensor for planetary rover absolute heading detection," *IEEE Trans. Robot. Autom.*, vol. 17, no. 6, pp. 939–947, Dec. 2001.
[37] S. Pfister, S. Roumeliotis, and J. Burdick, "Weighted line fitting algorithms for mobile robot map building and efficient data representation," in *Proc. IEEE Int. Conf. Robot. Autom.*, Taipei, Taiwan, R.O.C., Sep. 2003, pp. 1304–1311.
[38] N. Trawny and S. I. Roumeliotis, "A unified framework for nearby and distant landmarks in bearing-only SLAM," presented at the IEEE Int. Conf. Robot. Autom., Orlando, FL, May 2006.
[39] M. Bosse, R. Rikoski, J. Leonard, and S. Teller, "Vanishing points and 3D lines from omnidirectional video," in *Proc. Int. Conf. Image Process.*, Rochester, NY, Sep. 2002, pp. 513–516.
[40] P. S. Maybeck, *Stochastic Models, Estimation, and Control*, ser. Mathematics in Science and Engineering. New York: Academic, 1979, vol. 141–2.
[41] S. Julier and J. K. Uhlmann, "A counter example to the theory of simulataneous localization and map building," in *Proc. IEEE Int. Conf. Robot. Autom.*, Seoul, Korea, May 2001, pp. 4238–4243.
[42] J. A. Castellanos, J. Neira, and J. D. Tardos, "Limits to the consistency of EKF-based SLAM," presented at the 5th IFAC Symp. Intell. Auton. Veh., Lisbon, Portugal, Jul. 2004.
[43] P. Tabuada, G. J. Pappas, and P. Lima, "Feasible formations of multi-agent systems," in *Proc. Amer. Control Conf.*, Jun. 2001, pp. 56–61.
[44] A. I. Mourikis and S. I. Roumeliotis, "Optimal sensor scheduling for resource-constrained localization of mobile robot formations," *IEEE Trans. Robot.*, vol. 22, no. 4, Aug. 2006.
[45] ——, "Analysis of positioning uncertainty in reconfigurable networks of heterogeneous mobile robots," Dept. Comput. Sci., Univ. Minnesota, Minneapolis, 2003 [Online]. Available: www.cs.umn.edu/~mourikis/TR multi.pdf, Tech. Rep.
[46] T. Nishimura, "Error bounds of continuous Kalman filters and the application to orbit determination problems," *IEEE Trans. Aerosp. Electron. Syst.*, vol. AES-12, no. 3, pp. 267–275, Jun. 1967.
[47] D. Lerro and Y. Bar-Shalom, "Tracking with debiased consistent converted measurements versus EKF," *IEEE Trans. Aerosp. Electron. Syst.*, vol. 29, no. 7, pp. 1015–1022, Jul. 1993.
[48] B. Mohar, "The Laplacian spectrum of graphs," *Graph Theory, Combin., Appl.*, vol. 2, pp. 871–898, 1991.
[49] F. R. K. Chung, *Spectral Graph Theory*. Providence, RI: Amer. Math. Soc., 1997.
[50] S. Friedland and R. Nabben, "On cheeger-type inequalities for weighted graphs," *J. Graph Theory*, vol. 41, pp. 1–17, 2002.
[51] S. Boyd and L. Vandenberghe, *Convex Optimization*. Cambridge, U.K.: Cambridge Univ. Press, 2004.
[52] B. Hassibi, "Indefinite metric spaces in estimation, control and adaptive filtering," Ph.D. dissertation, Dept. Elect. Eng., Stanford Univ., Stanford, CA, Aug. 1996.

Anastasios I. Mourikis (S'04) received the Diploma of Electrical and Computer Engineering with honors from the University of Patras, Patras, Greece, in 2003. He is currently working toward the Ph.D. degree with the Department of Computer Science and Engineering (CSE), University of Minnesota, Minneapolis.

His research interests lie in the areas of localization in single- and multirobot systems, vision-aided inertial navigation, simultaneous localization and mapping, and structure from motion.

Mr. Mourikis is the recipient of the 2005 Excellence in Research Award Fellowship from the CSE Department, University of Minnesota.

Stergios I. Roumeliotis (M'02) received the Diploma in Electrical Engineering from the National Technical University of Athens, Athens, Greece, in 1995, and the M.S. and Ph.D. degrees in electrical engineering from the University of Southern California, Los Angeles, in 1997 and 2000, respectively.

From 2000 to 2002, he was a Postdoctoral Fellow with the California Institute of Technology, Pasadena. Since 2002, he has been an Assistant Professor with the Department of Computer Science and Engineering, University of Minnesota, Minneapolis. His research interests include inertial navigation of aerial and ground autonomous vehicles, fault detection and identification, and sensor networks. Recently, his research has focused on distributed estimation under communication and processing constraints and active sensing for reconfigurable networks of mobile sensors.

Dr. Roumeliotis is the recipient of the McKnight Land-Grant Professorship award and the NASA Tech Briefs award.